CRYSTAL GROWTH & DESIGN

Article

Study of Physicochemical and Explosive Properties of a 2,4,6-Trinitrotoluene/Aniline Cocrystal Solvate

Nadia S. Fondren, Zachary T. Fondren, Daniel K. Unruh, Amitesh Maiti, Anthony Frank Cozzolino, Yong Joon Lee, Louisa Jane Hope-Weeks, and Brandon L. Weeks

Cryst. Growth Des., **Just Accepted Manuscript** • DOI: 10.1021/acs.cgd.9b00779 • Publication Date (Web): 03 Dec 2019

Study of Physicochemical and Explosive Properties of a 2,4,6-Trinitrotoluene/Aniline Cocrystal Solvate

Nadia S. Fondren[†,#], Zachary T. Fondren[†,#], Daniel K. Unruh[§], Amitesh Maiti[‡], Anthony Cozzolino[§], Yong Joon Lee[†], Louisa Hope-Weeks[§], and Brandon L. Weeks[*,†]*

[†]Department of Chemical Engineering, Texas Tech University, Lubbock, TX 79409, USA

[‡]Department of Chemistry and Biochemistry, Texas Tech University, Lubbock, TX 79409, USA

[‡]Lawrence Livermore National Laboratory, Livermore, California 94551, USA

[§]Department of Chemistry & Biochemistry, Texas Tech University, Lubbock, Texas 79409, USA

* Corresponding author: brandon.weeks@ttu.edu

[#] The authors equally contributed to this work.

Abstract: In the development of crystal engineering and supramolecular chemistry, cocrystallization has been used as a way to develop novel explosives with tailored properties. We present a novel cocrystal solvate composed of TNT and aniline that exhibits unique physicochemical and explosive properties. X-ray diffraction studies reveal the crystallographic structure to contain TNT and aniline in a 1:1 molecular ratio. The crystals themselves exhibit a

vibrant, ruby red color which likely results due to a charge-transfer interaction between the overlapping π-orbitals of the aromatic rings. The most notable evidence for a charge-transfer complex is the appearance of a broad absorbance peak in the visible region which is not present in the spectrum of either pure component. Comparisons of the cocrystal solvate to that of pure TNT are conducted to determine thermodynamic and kinetic parameters using both experimental and theoretical techniques. The desolvation of aniline from the cocrystal solvate was also investigated using both *in situ* PXRD and AFM measurements to monitor changes in the crystal structure and surface topography, respectively.

1. Introduction

The process of cocrystallization occurs when two or more neutral species non-covalently interact to produce a crystalline solid consisting of each component in stoichiometric proportion (*e.g.* 1:1, 1:2, 1:3:1, *etc*.)[1]. The end result of cocrystallization, however, is a matter of debate[2] outside of certain vaguely accepted classifications such as multicomponent crystals, molecular complexes, *etc*.[3]. On one hand, researchers use the definition that a cocrystal is formed if, and only if, each of the individual components exist as crystalline solids under ambient conditions prior to cocrystallization[4–8] (*viz.* Desiraju[9]). On the other hand, some researchers refer to cocrystals in a broader sense in which they are simply defined as being the product of two or more species that have cocrystallized[1,10–14] (*viz.* Dunitz[15]). Solvates, for example, are defined as multi-component crystals containing at least one species that is liquid under ambient conditions. Many researchers maintain that the use of a distinguishing terminology is necessary when referring to these class of compounds (*e.g.* hydrates, solvates, or pseudopolymorphs[16–19]) since they tend to exhibit significant differences regarding certain physical properties (*e.g.* solubility, stability, storage,

and/or processing[20–22]). For all intents and purposes, it is of the author's opinion that solvates and hydrates are simply one of the many distinctions contained within a generalized definition of a cocrystal (*viz*. Stahly[23]). It appears that the most appropriate solution to this conundrum is likely via the route of compromise. Therefore, the results of this report will henceforth be referred to by the term "cocrystal solvate"[24].

The current and most common applications of explosives consist of mixing commercially manufactured energetic materials with varying proportions of polymers, metals, or other explosives to modify their bulk performance. Interestingly, the explosive compounds that are most widely used today were developed around or before World War II (*e.g.* TNT, PETN, HMX, RDX, *etc*.). Indeed, modern research has focused on developing new explosive materials although their industrial implementation has been mostly hindered due to concerns of their viable mass production relative to the cost of their synthetic precursor(s), explosive performance, safety to manufacture, storage stability, and, above all else, their tendency to detonate (*i.e.* sensitivity)[25]. CL-20 (*est.* 1987[26]) and FOX-7 (*est.* 1998[27]) are more recent hallmark examples of newly developed explosives that have achieved bulk commercialization. Since successful commercial production of new chemical explosives is historically rare, a significant amount of research has focused on finding ways to alter the performance of energetic compounds that are already manufactured in bulk. Examples include particle coating[28], amorphous stabilization[29], polymorph purification[30,31], and cocrystallization. Cocrystallization has been studied by energetics researchers in an attempt to analogously replicate the successes that have been achieved in pharmaceuticals research where, rather than drug solubility[32], the focus is shifted mainly towards alterations in sensitivity and, to a lesser extent, power[1,4,5,10,11,33–40].

2,4,6-Trinitrotoluene (TNT), the explosive compound investigated here, was originally used as a dyeing agent in the late 1800's and was the most commonly used conventional military explosive throughout the 20th century[25]. The reason that TNT was and continues to be so widely used can mostly be attributed to its low sensitivity, ease of manufacture, safety in handling, mold-casting ability with other explosives, and low toxicity[25]. Currently, TNT is rarely used alone but is more commonly found within composite mixtures containing other explosives[25].

TNT has been shown to mostly occur as either a monoclinic (more stable) or orthorhombic polymorph under ambient conditions[41,42]. Sherwood and co-workers reported that it was possible to reliably produce either polymorph depending on the solvent (*i.e.* relative solubility) that was used during the crystallization process[43]. While performing a comparable investigation related to the polymorphic crystallization of TNT in a wider array of different solvents[44], it was unexpectedly discovered that TNT and aniline cocrystallized to produce a cocrystal solvate with a ruby red appearance (Figure 1A,B). A similar red color transition is also observed in aniline solutions containing relatively high concentrations of TNT (Figure 1C). Other studies have shown that TNT interacts with certain amines in solution to produce a comparable red color change and is commonly used for colorimetric detection[45–51]. The underlying mechanism responsible for the observed color change in TNT/amine systems has been widely attributed to the formation of a suspected Meisenheimer complex. In general, a Meisenheimer complex refers to the formation of a covalent bond (Figure 2) that arises from a species' nucleophilic attraction towards the π-orbitals of an aromatic compound that is conjugated with electron withdrawing functional groups[46,52]. This mechanism is widely used in organic chemistry for reactions involving aromatic substitution and/or addition such as the conversion of trinitrobenzene to trinitrophenol[53]. In fact, Fant and co-workers[45] previously reported that TNT forms a Meisenheimer complex with aniline in the

presence of H_2O/acetone-d_6 on the basis of their carbon based nuclear magnetic resonance (CNMR) measurements.

However, the interaction of TNT with aniline in this report suggests the mechanism is better attributed to the formation of a charge-transfer complex. Beginning in the 1950s (*viz.* Mulliken[54–56]), there was a classical debate amongst researchers regarding the mechanism responsible for inducing the observed color changes in certain systems[57–59], and researchers went to great lengths to distinguish between charge-transfer and various other interactions such as ionic, hydrogen bonding, and Meisenheimer complexes[60–68]. Charge transfer complexes can be characterized as a special case of electron sharing between a donor and an acceptor in which two separate species become locally bound to each other through a transfer of electronic charge[54,55]. That is, an electron from either a lone pair (called "(*n*)-donors") or the π-orbitals of an aromatic compound (called "π-donors"), particularly those with an electron releasing group, can be donated to the empty orbitals of an acceptor[59]. Charge-transfer forces are typically comparable in magnitude to dispersion forces[55]. A comparative depiction of both a Meisenheimer and a charge-transfer complex is shown in Figure 2 for TNT and aniline. In general, charge transfer complexes can be characterized as follows[57,59]: an almost instantaneous change in color, a stoichiometric proportionality (*e.g.* 1:1 donor/acceptor), a broad absorption band in the visible spectrum, spectral shifts in the IR, intra- and intermolecular atomic spacing, and shifts in the nuclear magnetic resonance (NMR). Except for the NMR shifts, all of the aforementioned criteria are observed in the subsequent characterization of the TNT/aniline cocrystal solvate.

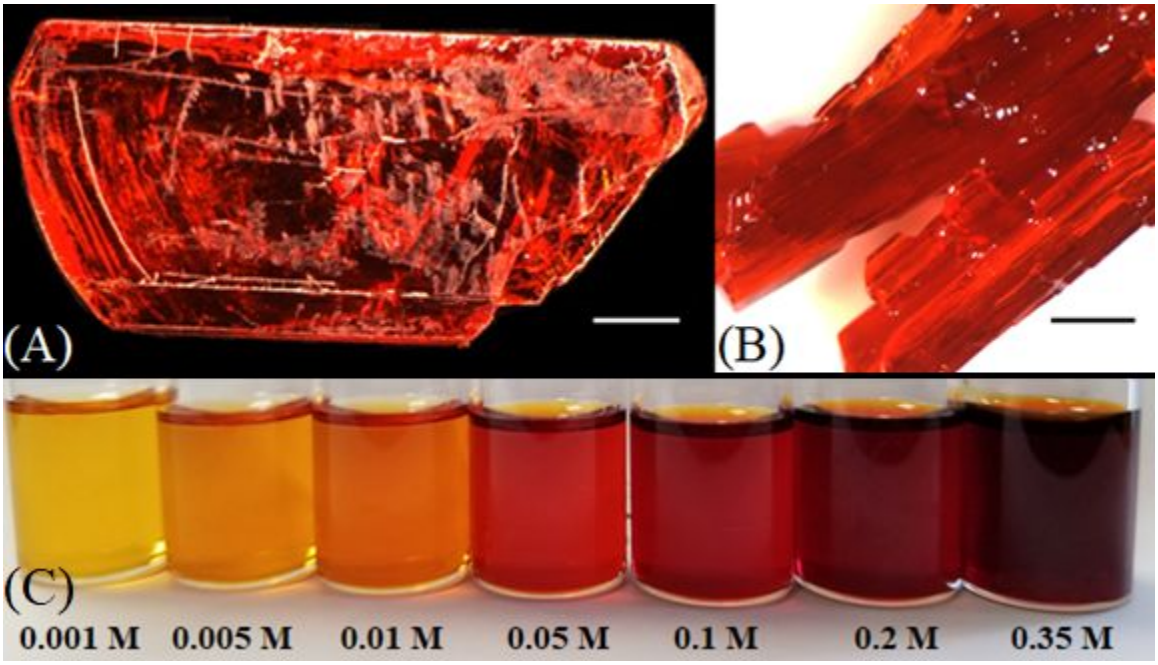

Figure 1. Macroscopic images of TNT/aniline cocrystal solvates grown with excess aniline at (A) room temperature (A) and 5 °C (B). The scale bar is approximately 2 mm. (C) Comparison of the progressive deepening in red color that occurs almost instantly within aniline solutions containing increasing concentrations of TNT.

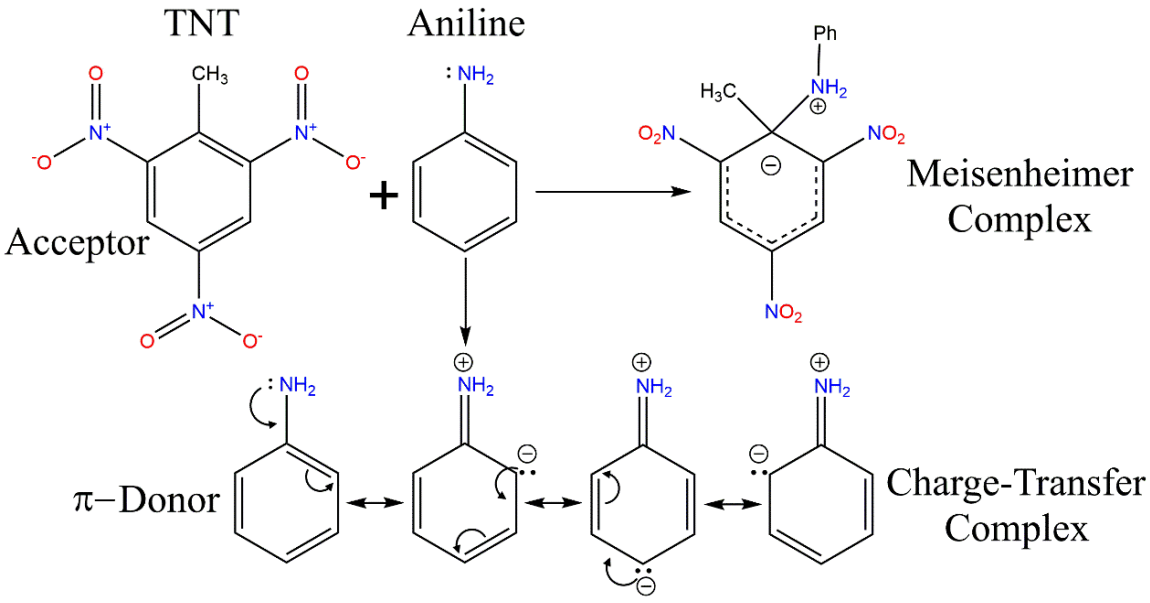

Figure 2. Comparison of the potential mechanisms in which TNT and aniline interact to produce the red color observed in the cocrystal solvate.

In this work, experimental and theoretical properties of the TNT/aniline complex are reported relative to that of pure TNT. Single crystal X-ray diffraction (SCXRD) studies were used to assess the structure and composition of the TNT/aniline cocrystal solvate. The thermal properties were investigated with both differential scanning calorimetry (DSC) and thermogravimetry (TG). Additionally, theoretical predictions of certain key explosive measures related to performance were determined using CHEETAH 8.0 software.

A notable observation of the cocrystals was that the vibrant red color fades over an extended period to ultimately exhibit a brownish yellow color characteristically observed in pure TNT. After complete discoloration, results obtained from IR spectroscopy suggests complete desolvation of aniline from within the solid material. PXRD was used to monitor the solid-state changes throughout the desolvation process, and it was later observed that this transformation could also be mapped along the exterior surface *in situ* with atomic force microscopy (AFM).

2. Experimental

2.1. Materials

All solvents (aniline, acetone, hexanes, and acetonitrile) were ACS grade. TNT flake was obtained from Dyna energetics. TNT flake was purified via solvent-antisolvent precipitation[44] using 1 ml of acetone and excess water followed by thorough drying with vacuum filtration. The purity of TNT was then confirmed to be 99.67% using HPLC (BDS hypersil C-18, column size: 150 x 2.1 mm – Note: samples were dissolved in 25/75% acetonitrile/water and analyzed using a 200 µl min^{-1} flow).

2.2. Preparation of the Cocrystal Solvate

Approximately 80 mg of the purified TNT crystals were dissolved in 1 ml of aniline (slightly below the saturation limit[69]) in a 2-dram vial. The prepared solutions were then allowed to crystallize in an open vial at either room temperature or 5 °C. After careful removal of the supernatant, crystal samples were quickly dried with tissue paper and immediately stored in a sealed, air-tight container. The samples can also be dried using a vacuum filter apparatus and rinsing with a small amount of ethanol. Once dried and sealed in an air-tight vial, the cocrystal solvate samples were remarkably stable for weeks to months such that there was not any visible discoloration. Herein, all results stem from crystal samples obtained using this procedure since it gave the greatest likelihood of producing large, single crystals. However, two additional sample preparation procedures were later discovered and are described in the supporting information (SI) (SI-A – Section/Figure S1).

2.3. Optical Microscopy

Macroscopic images of select cocrystals were obtained with an optical microscope (Olympus SZH) and camera (Olympus Q-color 3).

2.4. Single Crystal X-ray Diffraction (SCXRD)

SCXRD measurements were performed using a Bruker three circle diffractometer with an APEX II CCD detector. Operation was performed at either -173 °C or 25 °C using 1500 W (50 kV, 30 mA) graphite-filtered molybdenum Kα radiation (λ = 0.71073 Å). Samples were precoated with poly(isobutylene). Assessment of unit cell information was performed using an Omega scan method with both a 20 second exposure time and 0.5° rotation per frame. Efforts were made to ensure prevention of translational rotation during imaging.

After data collection, the unit cell was re-determined using a subset of the full data collection. Errors in the intensity (Lorentz force/polarization/background radiation) were corrected using

Bruker APEX 3 software. A semi-empirical correction concerning absorption was applied using *SADABS* software[70]. *SHELXL (2014)*[71] software was used for the solution and refinement of the crystal structure. Hydrogen atoms bound to carbon and nitrogen atoms were identified from the difference Fourier map and geometrically constrained using the appropriate AFIX or DFIX commands.

2.5. Powder X-ray Diffraction Analysis (PXRD)

Powder diffraction patterns were obtained on a Rigaku Ultima III instrument operated at 1760 W (40 kV, 44 mA) using germanium-filtered copper Kα radiation (λ =1.5418 Å). The samples were prepared in a standard sample holder, and the data was collected in reflection mode with the 2θ scan angles ranging from 5-50°. For all measurements, the step size was 0.2° and the scan time was varied between 1-3 degrees per minute. Diffractograms were processed using the software packing JADE v9.1.1.

2.6. Diffuse Reflectance

Diffuse reflectance measurements were obtained with a Stellarnet Silver Nova spectrometer (CCD detector). The spectrometer was externally connected to separate tungsten (visible) and deuterium (ultraviolet) light sources (StellarNet, Inc. SL1 and SL3, respectively) that were coupled through a fiber optic cable to the diffuse reflectance probe (StellarNet, Inc.) that was placed over the sample in an enclosed chamber. A dark background and a 100% reflectance baseline relative to a barium sulfate standard were collected before each sample measurement. Samples were then ground into a powder and placed on top of the barium sulfate standard for each measurement. Data collection was performed using Spectragryph software (version 1.2.13) with a 2500 ms integration time and a 20-scan average.

2.7. Infrared (IR) Spectroscopy

IR spectra (Nicolet iS10 FTIR) were collected using attenuated total reflection (ATR) (diamond attachment - Thermo Fisher Scientific) over the wavenumber range 4000 – 400 cm^{-1} with a 1 cm^{-1} resolution.

2.8. Differential Scanning Calorimetry (DSC)

For DSC measurements (Model Q20 RSC90 – TA instruments), the thermal response (W g^{-1}) of ~3-5 mg of crystal sample was measured for two different cases using nitrogen purge gas at a flow rate of 50 ml min^{-1}. *Case 1:* Crystals samples of TNT or the TNT/aniline cocrystal solvate were hermetically sealed in a DSC pan and measured at a heating rate of 20 ^oC min^{-1} over the temperature range 20 – 300 ^oC (Figure 7). *Case 2:* A TNT/aniline cocrystal solvate sample was equally heated and cooled at a rate of 5 ^oC min^{-1} in an open pan for five consecutive cycles in the range of 20 – 120 ^oC. The mass of the pan was accurately weighed both before and after each respective cycle (Figure 9).

2.9. Thermogravimetry (TG)

For TG measurements (model Q50 – TA instruments), the rate of mass-loss was measured non-isothermally with a heating rate of 20 ^oC min^{-1}. Nitrogen was used as the purge gas with a sample flow rate of 90 ml min^{-1} and a balance flow rate of 10 ml min^{-1}. The mass of sample used was 30.0 ± 0.5 mg.

2.10. Atomic Force Microscopy (AFM)

The time-dependent surface transformation due to air exposure was monitored isothermally at 35.0 ± 0.1 ^oC via repetitive site-specific scanning of a single region on the exterior surface using contact mode AFM (Bruker Multimode 8 with heating stage attachment; imaging software – Bruker Nanoscope Analysis 1.7). All scan sizes were 20 x 20 μm^2 and scan rates were 2 Hz. Image processing and analysis were performed with Scanning Probe Image Processor (SPIP) v6.7.0

(Image Metrology). AFM tip parameters: company – Bruker; material – silicon nitride; frequency – 23 kHz; nominal spring constant – 0.12 N m^{-1}; tip radius – 10 nm.

3. Results and Discussion

3.1. Crystal Structure

The packing arrangement of the molecules within the structure and the corresponding crystallographic data are shown in Figure 3 and Table 1, respectively. PXRD diffractograms of a TNT/aniline cocrystal solvate and pure TNT (orthorhombic polymorph) are shown in Figure 4. The SCXRD results indicate that the TNT/aniline cocrystal solvate crystallizes in the orthorhombic space group *Pnma*. Within the unit cell, TNT and aniline are paired in a stoichiometric ratio of 1:1 with weak hydrogen bonding interactions between the amine and the *ortho* nitro groups of TNT (N···O = 3.205(1) Å). Their aromatic rings are co-planar along the a- and b-axes, and each coplanar pair of TNT/aniline molecules is oppositely paired with another set of coplanar TNT/aniline molecules along the c-axis. In the following discussion, "pairs" are distinguished as being either "coplanar" or "opposite". In each opposite pair, the conformation of aniline is such that its amine nitrogen is positioned along the c-axis opposite from the tertiary carbon atom (C_1) in TNT's phenyl ring. This places the amine group centrally in-between TNT's nitro groups at the *ortho*- positions. This results in twist angles in the nitro groups of TNT (relative to the aromatic ring) to be approximately 40° at both of the *ortho*- positions and 0.1° at the *para*- position.

Starting from the origin of Figure 3A and moving upwards between coplanar pairs along the a-axis, there are four "groups" of opposite pairs and four "groups" of coplanar pairs. The dashed lines in Figure 3B between the *ortho*- carbons of aniline and *meta*- carbon of TNT, respectively, indicate a close stacking region in which the sum of the distances between these positions on the respective phenyl rings are slightly less than the sum of the Van der Waal radii (3.40 Å). However,

the separation distance between opposite pairs is not the same. The distance between aniline's phenyl ring carbon that is attached to the amine (C_1) and a 10-atom centroid within TNT (consisting of all of the carbon and nitrogen atoms) was used to approximate the ring separation distance (using CCDC's Mercury software ver. 4.1.3) and were measured to be 3.377(1) Å at the $1^{st}/4^{th}$ positions and 3.325(1) Å at the $2^{nd}/3^{rd}$ positions. Similar ring separation distances have been reported in cocrystal systems where the formation of a charge-transfer complex was observed to occur between π-orbitals[72–75].

Several different intermolecular interactions appear to exist based on the crystal structure. The close stacking of the aromatic rings that occurs between TNT and aniline in a 1:1 ratio is consistent with the formation of a charge-transfer complex in which π-π^* electron sharing occurs between the highest occupied molecular orbital (HOMO) in aniline (the donor) and the lowest unoccupied molecular orbital (LUMO) in TNT (the acceptor) via π-orbital overlap in the opposite pairs. The source of electron contribution in aniline likely results from delocalization of the lone electron pair in the amine group into the phenyl ring (Figure 2) to yield an aniline cation. In this case, it is predicted that the amine bond to the phenyl carbon (C_1) would be slightly reduced. This is supported by the crystallographic data in which our reported C_1-N bond length of 1.370(2) Å is slightly less than the experimental length previously reported[76] (1.402(2) Å) and is in agreement with the theoretical prediction of a coplanar amine formation in aniline[77] (1.378 Å). However, this is slightly more than the theoretical prediction[78] for a carbon nitrogen double bond length of 1.332 Å.

In addition to the π-interactions, there is also a significant amount of Van der Waal's interactions between the nitro groups of neighboring TNT molecules in the adjacent positions. Each oxygen atom of the nitro groups at the *ortho*- positions exhibit at least one interaction with an adjacent

nitro group where the distance is slightly less (2.888(1) Å) than the sum of the Van der Waal radii (3.04 Å). The specific oxygen atom in the *ortho*- nitro group that has two interactions is the one that is closest in proximity along the a-axis, but the exact vector direction (predominantly along the b-axis) varies based on the relative orientations of the two interacting *ortho*- and *para*- nitro groups.

The SCXRD measurements at 25 °C were conducted for assessing the thermal expansion and ambient stability of the cocrystal solvate. However, due to the decomposition of the crystal at this temperature, only unit cell data were collected. Sample measurements at 25 °C (marked with an * in Table 1) show an increase in the lattice length parameters a, b, and c by approximately 0.7, 1.6, and 2.8 %, respectively, and an overall volume expansion of roughly 5% compared to measurements at -173 °C.

Geometry optimization of the experimentally determined structure using first-principles periodic density functional theory (DFT) under constrained cell and space group symmetry showed insignificant changes to the positions of all atoms in the unit cell, both non-hydrogen and hydrogen, thus verifying the correctness of positional assignment and structural stability. The DFT calculations[79] were performed using the code "DMol^3" in which we employed the gradient-corrected PBE exchange-correlation function[80] with a double-numeric-polarized (DNP) basis set on a "fine" numerical grid and a real-space global cutoff of 4.0 Å. Accurate Brillouin-zone sampling was ensured throughout the summation over a finite set of K-points chosen according to the Monkhorst-Pack scheme[81] with a grid spacing of 0.05 Å-1.

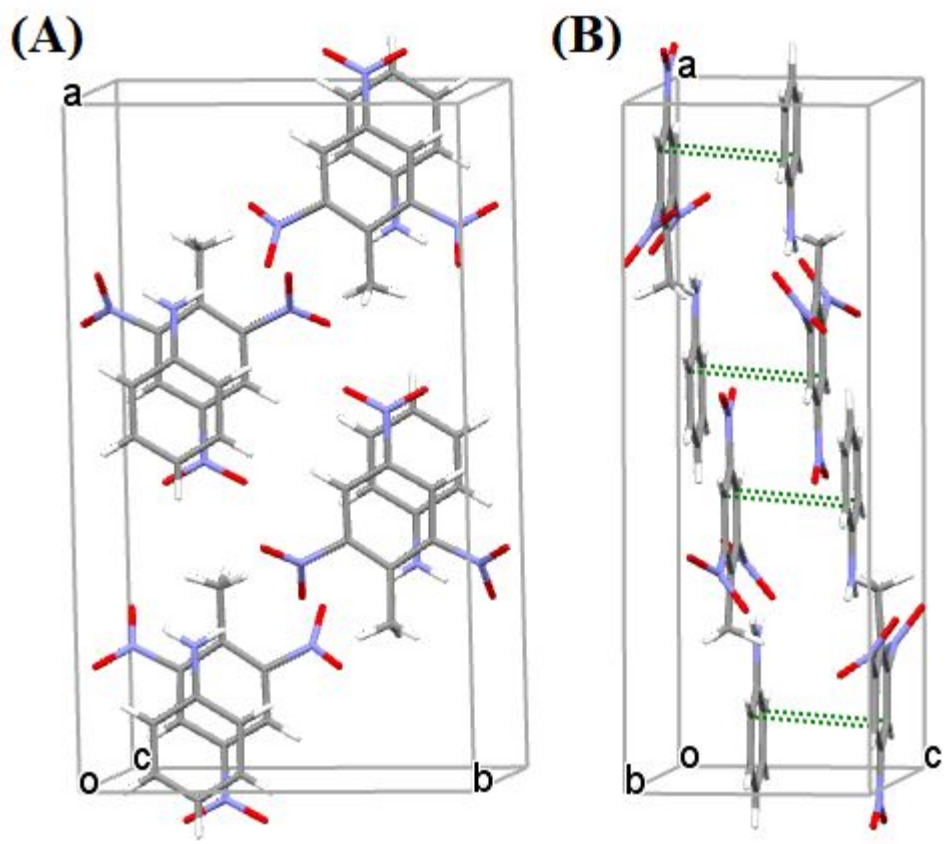

Figure 3. SCXRD representation of the packing arrangement and orientation of TNT and aniline present within the cocrystal solvate as viewed along the c-axis (A) and b-axis (B). The green dashed lines in (B) indicate intermolecular distances that are less than the sum of the Van der Waal radii. The depictions were created using the CCDC's Mercury software ver. 4.1.3. (Note: carbon – grey; nitrogen – blue; oxygen – red; hydrogen – white)

Table 1. Crystal data and structure refinement for the TNT/aniline cocrystal solvate as measured at -173 and 25 ^{o}C.

Structural parameters	**Parameter values**
Empirical formula	$C_{13}H_{12}N_4O_6$
Formula weight (g mol^{-1})	320.27
Temperature (^{o}C)	-173

Crystal system	Orthorhombic	
Stoichiometry	1:1	
Space group	*Pnma*	
a (Å)	18.726(2)	18.86*
b (Å)	10.9375(13)	11.11*
c (Å)	6.7023(8)	6.89*
α (deg.)	90	90*
β (deg.)	90	90*
γ (deg.)	90	90*
Volume (Å^3)	1372.7(3)	1443.68*
Number of molecules in asymmetric unit, Z	4	
Absorption coefficient, m (mm^{-1})	0.125	
F(000)	664	
Crystal size (mm^3)	0.46 × 0.34 × 0.28	
Crystal Density[a] (g cm^{-3})	1.550	
Index ranges	$-24 \le h \le 24$, $-14 \le k \le 14$, $-8 \le l \le 8$	
Reflection collected	15166	
Independent reflections	1599 [R(int.) = 0.0341]	
Data/restraints/parameters	1599/2/120	
Goodness-of-fit on F^2	1.066	
Final R indexes ($I \ge 2\sigma(I)$)	R_1 = 0.0305, wR_2 = 0.0924	
Final R indexes (all data)	R_1 = 0.0340, wR_2 = 0.0965	
Largest diff. peak/hole/e (Å^{-3})	0.243/-0.341	
Theta range for data collection (deg.)	2.175 to 27.116	

[a] Crystal density of TNT[82] = monoclinic: 1.713 g cm^{-3} at -173 °C
orthorhombic: 1.704 g cm^{-3} at -150 °C

*Values determined at 25 °C

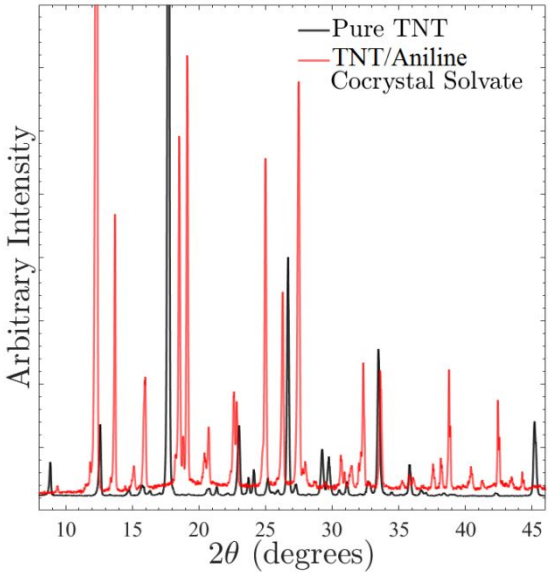

Figure 4. PXRD patterns for an orthorhombic crystal of pure TNT (black) and a TNT/aniline cocrystal solvate (red).

3.2. Optical Properties

A key, distinguishing feature frequently observed in charge-transfer complexes is the existence of a broad, optical absorbance band in the visible region[57,59,72,75,83–85]. The diffuse reflectance absorbance spectra for pure TNT and a TNT/aniline cocrystal solvate are shown in Figure 5. As can be seen for the cocrystal solvate, there is a new absorbance peak that begins at approximately 600 nm and has a maximum absorbance around 495 nm. The difference between the approximate onsets for the lower-energy spectral absorbances (*e.g.* ~450 nm in TNT) is approximately 150 nm. This result is consistent with the red visual appearance in the cocrystal solvate occurring due to formation of a charge-transfer complex between TNT and aniline. Note: Aniline (liquid) begins to weakly absorb at around 500 nm and begins to strongly absorb at ~320 nm (SI-A – Section/Figure S2).

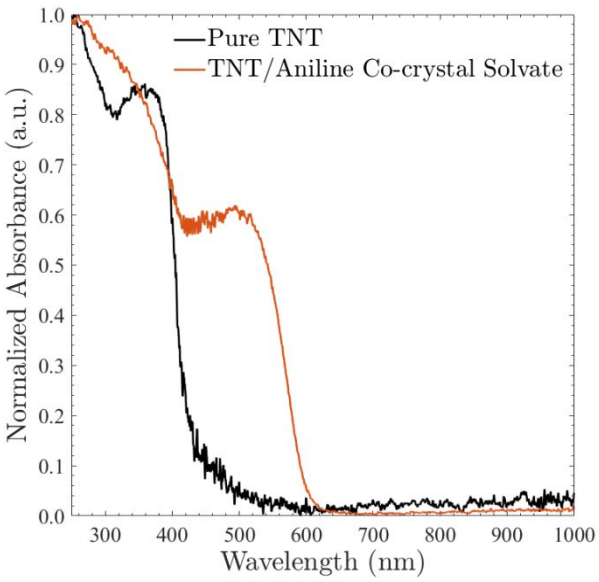

Figure 5. Diffuse reflectance absorbance spectra of pure TNT (black) and a TNT/aniline cocrystal solvate (red). The onset of spectral absorbance is redshifted in the cocrystal solvate (*e.g.* ~450 → ~600 nm) and exhibits a new peak whose maximum absorbance is around 495 nm. This result is consistent with the formation of a charge-transfer complex between TNT and aniline.

The IR absorbance spectra of TNT, aniline, and the cocrystal solvate are shown in Figure 6. In addition, a superposition of the IR absorbances for both of the pure components is overlaid onto the cocrystal solvate spectra, and the absorbance spectrum of a cocrystal solvate sample after exposure to an open-air environment for 24 hours is overlaid onto the pure TNT spectrum. The vibrational assignments in the IR spectra have been previously detailed for both TNT[86] and aniline[87,88], and the following discussion is based on their work. The three peaks >3100 cm^{-1} in the cocrystal solvate spectra are the most obvious indicators of aniline's presence within the cocrystal solvate since they do not appear in TNT's spectrum. In aniline, the peaks at 3428 and 3350 cm^{-1} are assigned to the asymmetric and symmetric stretches of $-NH_2$, respectively. In the cocrystal solvate, these stretches have been blue-shifted to 3489 and 3393 cm^{-1} ($\Delta\nu$ = -61 and -43 cm^{-1}), respectively. The most reasonable explanation for the shifting of these two peaks to higher

frequencies is that aniline experiences an extensive reduction in hydrogen bonding in the cocrystal solvate. Specifically, the characteristic wavenumber region for the $-NH_2$ functional group is between 3300-3000 cm^{-1} when hydrogen bonded and 3550-3420 cm^{-1} without hydrogen bonding[89]. The nearest neighbor distance between amine groups for two aniline molecules (*i.e.* $H_2N\cdots NH_2$) within the crystal structure of the cocrystal solvate (Figure 3) is 6.695(1) Å which is too large for there to be any appreciable hydrogen bonding occurring between amine groups. However, there is potential for hydrogen bonding between aniline's amine group and TNT's *ortho*-nitro groups since their nearest neighbor distance (along the b-axis) is 3.496(1) Å (*e.g.* O-N-$O^{-}\cdots NH_2$) although the hydrogen bond strength between two amines is significantly greater than an amine with a nitro group.

Characterization of the remaining peak shifts is problematic since it requires identifying the shifts in the parent intensities that are in a region where there is a combined presence of features that are similar in both aniline and TNT. That is, for the frequencies < 1600 cm^{-1}, most of the peak intensities are related to the vibrational modes of the aromatic ring features (*e.g.* 3-dimemsional symmetric/asymmetric stretching/bending/breathing/*etc.* and substituent related effects), and the convoluted, overlapping intensities of the peaks in this region makes it difficult to confidently assign peaks that have shifted in the cocrystal solvate spectrum with respect to the pure components. For example, the sharp cocrystal solvate peak at 3110 cm^{-1} is either related to the superposition of overtones for two different symmetric ring stretches in aniline which occur at ~1500 and ~1600 cm^{-1} (which are convoluted with TNT's nitro group and CC ring stretches, respectively), a peak-shifted superposition of the CH ring stretches in TNT that occur at 3095, 3084, and 3055 cm^{-1}, or a combination of both. In either case, there would be missing peak assignments in this region relative to the pure components and the cocrystal solvate. Additional

work is warranted to fully assign all of TNT and aniline's vibrational modes in the IR spectrum of the TNT/aniline cocrystal solvate. However, this may be difficult since it is typically achieved based on comparisons of peak locations after changes are made to the substituents (*e.g.* deuteration or group substitution)[86,87]. Furthermore, further characterization of the charge-transfer interaction based on inspection of the IR spectra is also difficult since it is typically assessed based on variations in the electron affinity of the acceptor (*e.g.* fluorination)[73]. In either case, it is uncertain as to whether a cocrystal solvate variant would still result after substantial changes are made to either the donor or acceptor.

However, there are some obvious features in the cocrystal solvate spectrum that are worth mentioning. For aniline, the peak at 1271 cm^{-1} appears to be blue-shifted to 1298 cm^{-1} ($\Delta\nu$ = 28 cm^{-1}) and is assigned to a symmetric ring stretch that is sensitive to the substituent since it involves considerable C-N stretching[87]. A similar blue-shifted peak difference was observed in the case of deuterated aniline-ND_2[87]. A shift of this peak is consistent with the mechanism of a charge-transfer complex since significant changes in the stretching mode between the ring and the amine group are expected. For TNT, many of the peaks involving the CNO vibrational modes do not appear in the cocrystal solvate spectrum. Specifically, the TNT peaks at 759, 769, 733, 716, 667, and 662 cm^{-1} are all, at least, assigned to a CNO bend[86]. The only one of these peaks that is clearly observed in the cocrystal solvate spectrum occurs at 720 cm^{-1} (appears to have a small shoulder). Pure TNT has been previously shown to have a total of six different nitro group twist angles in its crystal structure where the twist angles are essentially the same in both polymorphs. As mentioned earlier, TNT has only two different nitro group twist angles in the cocrystal solvate where one is co-planar with the ring. Based on this, a reduction in the number of CNO bends in TNT's vibrational spectrum is expected.

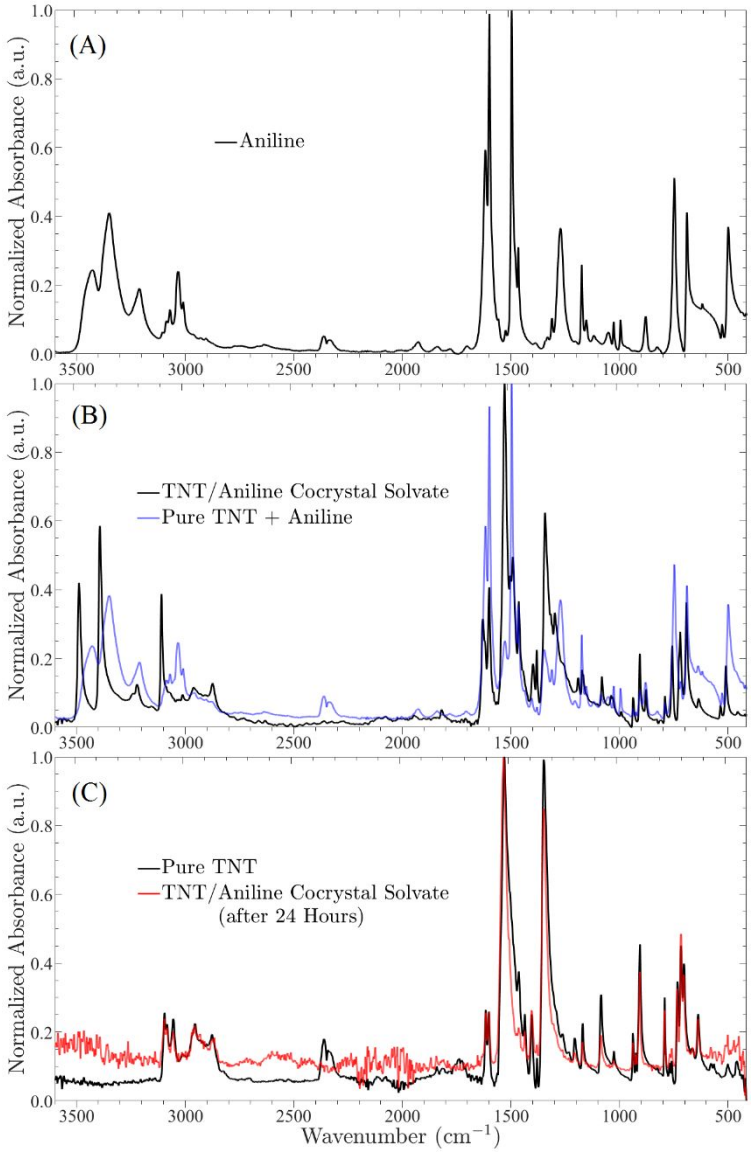

Figure 6. ATR-FTIR transmittance spectra of liquid aniline (A), a freshly prepared TNT/aniline cocrystal solvate (B), and a pure TNT crystal produced from toluene via antisolvent precipitation with water (C). A superposition of the TNT and aniline absorbances shown, respectively, in (A) and (C) are overlaid (blue) onto the cocrystal solvate spectra in (B), and the spectrum of a cocrystal solvate sample after exposure to air for 24 hours (*i.e.* complete discoloration from red to yellow) is overlaid (red) onto the pure TNT spectrum in (C). Note: The peaks at ~2350 cm^{-1} occur due to atmospheric carbon dioxide.

3.3. Thermodynamic Properties

DSC traces (hermetically sealed) for crystalline samples of either pure TNT or TNT/aniline are shown in Figure 7. The thermal response shows significant differences with regards to the phase-change temperatures. The onset melting endotherm of the TNT/aniline cocrystal solvate is seen to occur around 85 °C which is approximately 5 °C higher than the melting endotherm of pure TNT at 80 °C. Note: The melting point of the pure sample is in excellent agreement with previous reports[90] (80.8 °C). Additionally, the required heat of melting was also found to be higher (114.5 J g^{-1}) relative to the pure TNT crystal (105.9 J g^{-1}). For the second observable endotherm, the maximum heat flow of the pure TNT crystal mostly occurs as a wide, single peak centered around 255 °C. This endotherm is likely related to the decomposition of TNT which is reported[91] to begin occurring around 190 – 200 °C. For the case of the cocrystal solvate, there are two distinct endothermic peaks beyond melting that were observed at ~191 °C (onset) and 240 °C (central maximum), respectively. The nature of the first endotherm around 191 °C is most likely related to the evaporation of aniline (boiling point[92]: 184.5 °C). The second endotherm at 240 °C is also likely related to the decomposition of the remaining TNT after aniline has completely evaporated.

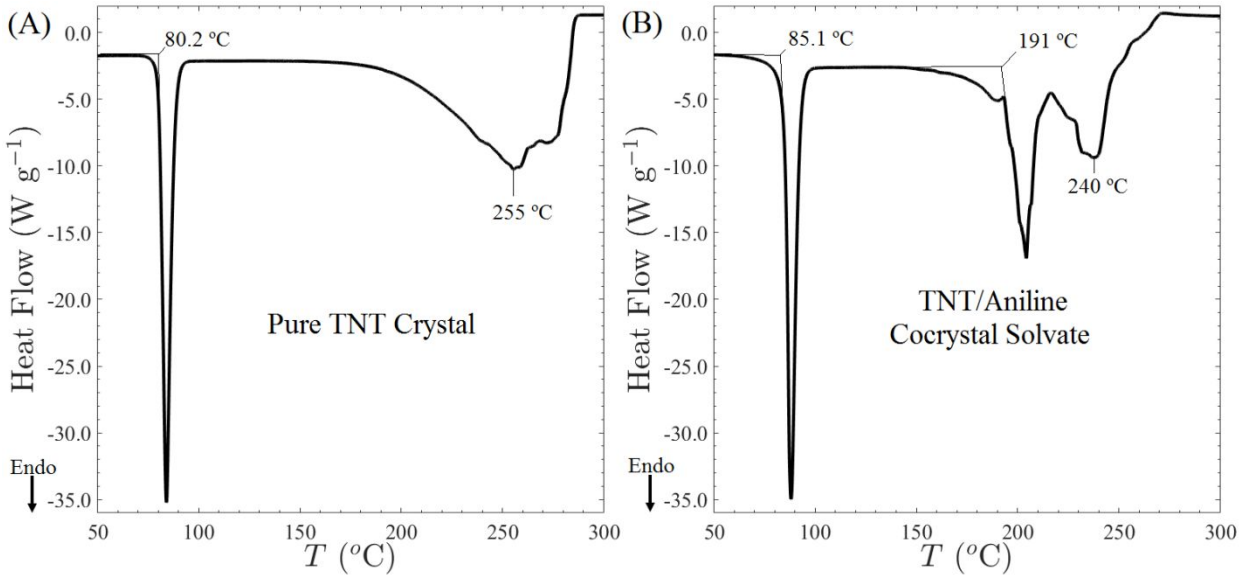

Figure 7. Experimental DSC traces of a pure TNT crystal (A) and a TNT/aniline cocrystal solvate (B) using a heating rate of 20 ^{o}C min^{-1}.

3.4. Aniline Desolvation

The desolvation of aniline from within the cocrystal solvate poses an important concern regarding both the thermal stability and shelf-life. Discoloration of the cocrystal solvate upon prolonged exposure in open air suggests aniline slowly leaves the crystal sample (*i.e.* desolvation) even at room temperature (

Figure **8**A). Red discoloration did not appreciably occur in samples that were sealed in a vial. The most likely reason for this is that the aniline vapor becomes saturated in a small volume which prevents further desolvation. Furthermore, it was observed that complete discoloration of the cocrystal solvate's red surface typically takes a maximum of 10 hours at ambient conditions depending on the crystal's size and shape. A macroscopic progression of this process is shown in

Figure **8**B. Obviously, the regression of the cocrystal solvate due to the desolvation of aniline is directly related to the long-term stability of these crystals if stored in open air. Hence, understanding the fundamental mechanism of its occurrence could assist in controlling the kinetics of the desolvation process and potentially improving the long-term storage.

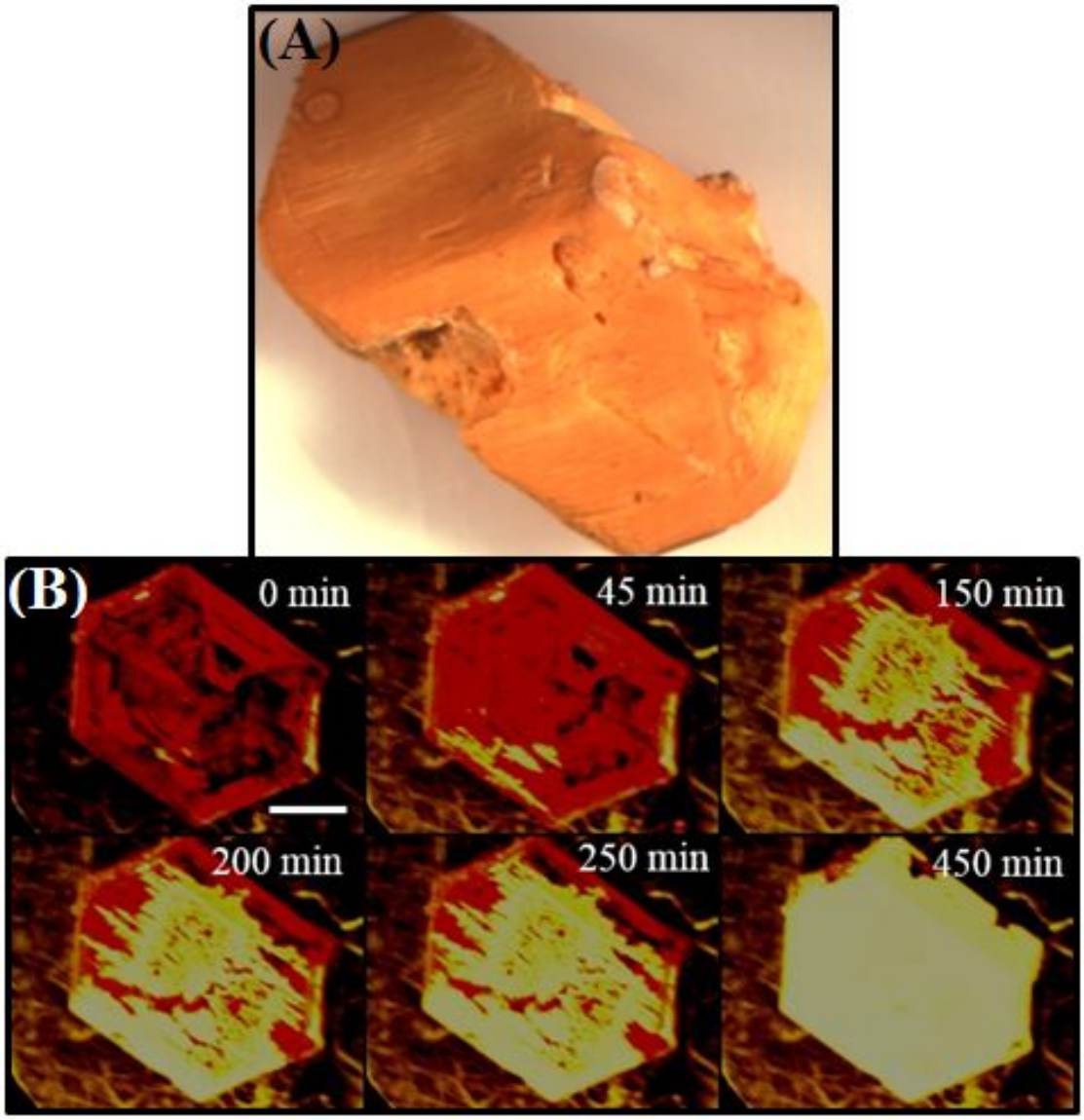

Figure 8. (A) Discoloration of the TNT/aniline cocrystal solvate after exposure to air (> 24 hours). The visual appearance of the crystal suggests that only TNT remains since pure crystals are typically brownish-yellow in appearance. (B) Macroscopic progression of the discoloration at the surface over a 9-hour period. The scale bar is 1 mm (images were taken with an optical microscope).

3.4.1. Desolvation due to Heating

A series of DSC measurements (Figure 9) were conducted in which a cocrystal solvate sample was subjected to multiple open-pan heating cycles (slightly above the melting point), and the mass was measured after each cycle following recrystallization (*i.e.* after cooling to room temperature). For the first heating cycle, there is a relative increase in the melting endotherm that is comparable to the result in Figure 7. However, the second cycle and beyond display a single endotherm located precisely at the melting temperature expected in pure TNT. The inset of Figure 9 shows that approximately 30% of the cocrystal solvate's mass disappeared after the first heating cycle. The change in the mass then appears to be relatively constant for all of the remaining heating cycles (*i.e.* due to TNT sublimation/evaporation). This suggests complete evaporation of aniline within the cocrystal solvate upon heating to the melting point in an open-pan setting. In the 2nd and 3rd cycles, the shoulder (*e.g.* 77-78 °C) that precedes melting is due to a phase-change in TNT from the orthorhombic to the monoclinic polymorph[41,44], but it does not imply that the recrystallized sample was purely orthorhombic. The lack of this shoulder in the 4th cycle does suggest, however, that the sample recrystallized exclusively as the monoclinic polymorph. Recrystallization did not occur after the 4th cycle.

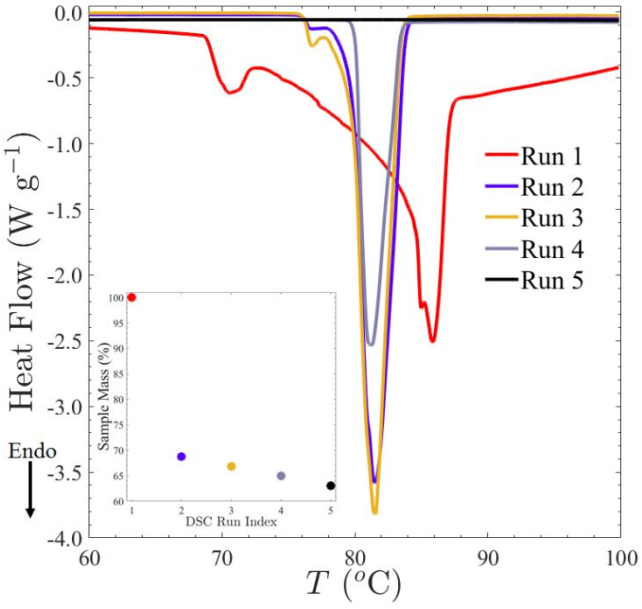

Figure 9. DSC traces (open-pan) for the same TNT/aniline cocrystal solvate sample after undergoing multiple heating and cooling (not shown) cycles up to slightly above the melting temperature. (Inset) The mass of the sample was subsequently measured after each respective cycle in which >30% was lost after the first run. The heating and cooling rates shown were both 5 ^{o}C min^{-1}.

TG measurements were also employed to further characterize the mass loss upon heating (Figure 10). The results show a progressive reduction in mass up to approximately 30% after heating from 50 to 100 ^{o}C. Analysis of a pure TNT crystal using the same TG conditions showed no significant reduction in mass (not shown). Furthermore, the mass percentage of aniline that would be present in a 1:1 molar ratio with TNT would be 29.1%. Hence, evidence suggests that aniline evaporates completely from the interior of the cocrystal solvate upon melting in an open atmosphere.

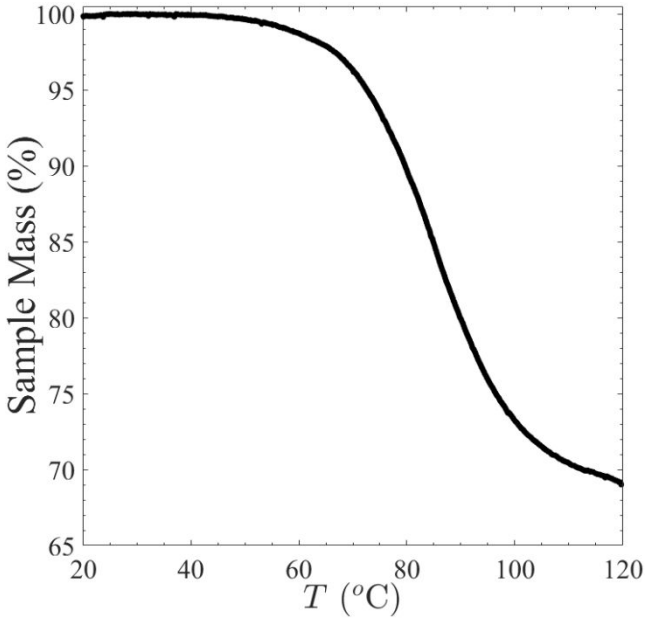

Figure 10. Non-isothermal TG results demonstrating the decrease in mass of a TNT/aniline cocrystal solvate sample when heated beyond the melting temperature. The heating rate was 20 ^{o}C min^{-1}. Note: For 1:1 molar mixture of the two, aniline constitutes ~29% of the mass.

3.4.2. Crystal Structure Changes under Ambient Conditions

PXRD was used to monitor the solid material during the desolvation process under ambient conditions[93]. It is important note that the cocrystal solvate sample, over the course of these measurements, was not mixed or perturbed in any way after it was loaded into the sample holder, and the relative peak intensities for the cocrystal solvate are potentially misleading due to orientation bias. Furthermore, the sample portion at the bottom of the sample holder likely underwent desolvation much slower than the upper layer portion that was exposed to open air, and the actual amount of time required for the conversion of the cocrystal solvate to pure TNT *in situ* (*e.g.* a single crystal left out on a benchtop) is likely less than it would be in the subsequent discussion since it would not be in a compact state that impairs the desolvation of aniline below the outermost sample surface.

Referring to Figure 11, the qualitative extent of crystal transformation due to aniline's desolvation, overall, does not appear visually significant until after 10 hours. However, new peaks representing the orthorhombic polymorph of TNT are weakly visible at 2θ angles of approximately 12.6°, 16.3°, 17.7°, 23.7°, 24.1°, 29.3° and 29.9° after the first 5 hours. As time progresses, the peak intensities for the cocrystal solvate decrease while the peaks intensities for TNT continue to increase. After 93 hours, the cocrystal solvate peaks at 12.4°, 18.7°, and 26.2° are nearly reduced to background, while the remaining peaks at 12.6°, 15.7°, 16.3°, 17.0° (weak intensity), 17.7°, 20.7°, 21.3° (weak intensity), 23.0° (most intense TNT peak), 23.7°, 24.1°, 26.0°, 26.7°, 27.3°, 29.3°, and 29.9° match with the orthorhombic polymorph for TNT, albeit with peak intensities with preferred orientation due to the *in situ* crystal growth of TNT in the sample holder (see SI-A – Section S3 for a higher resolution comparison).

Reitveld refinement was used to model the crystal structure transformation in the TNT/aniline cocrystal solvate as the overall composition of the PXRD sample transitioned towards having a diffraction pattern whose characteristics were more similar to that of pure TNT. We found that the general quality of the fit was improved by modeling the cocrystal solvate transition relative to two criteria: the orthorhombic polymorph of TNT and an amorphous contribution. The physical interpretation of the amorphous contribution is that the cocrystal solvate transitions through an amorphous phase before recrystallizing as TNT. The results of the Reitveld refinement are shown in Figure 11B, and complete details of the analysis are provided in the SI (SI-B – Section S4).

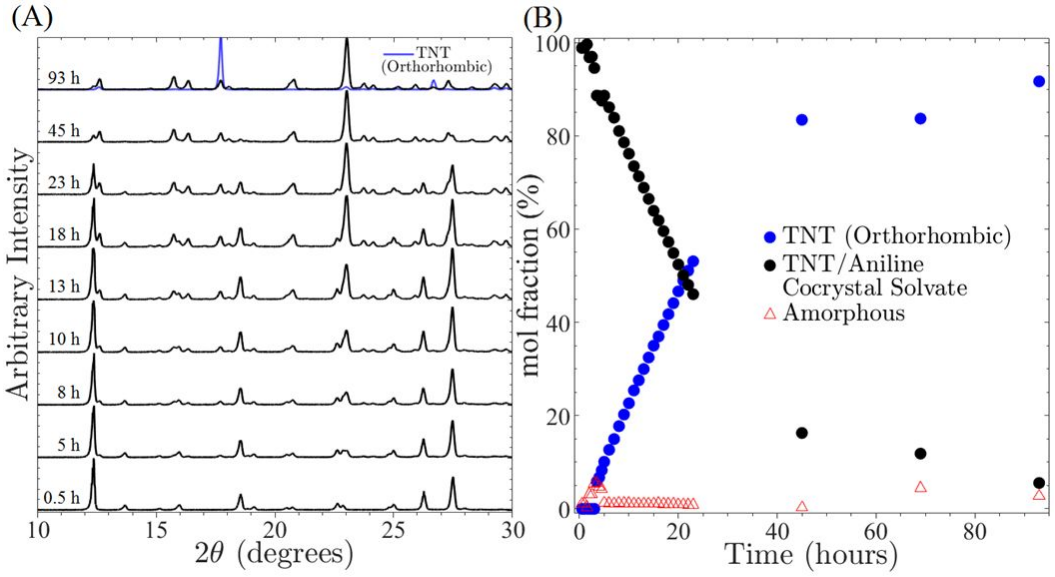

Figure 11. (A) A series of PXRD diffractograms of the TNT/aniline cocrystal solvate taken over time to monitor changes in the crystal structure under ambient conditions. (B) Time-dependent change in the crystal character as the cocrystal solvate converts into pure TNT due to aniline desolvation. The % composition was assessed by Rietveld analysis using the co-crystal solvate and the orthorhombic TNT polymorph as model patterns. During the analysis, it was determined that a small, amorphous component was also present throughout the crystal transition. Note: To demonstrate the conversion of the cocrystal solvate to TNT under ambient conditions, the sample

was not repacked between measurements. This resulted in preferred orientation of the TNT crystals and slowed the conversion of the bottom portion of the sample.

3.4.3. Changes in Surface Morphology

In-situ AFM was used to observe the microstructural morphology change over time in a single crystal of a TNT/aniline cocrystal solvate during isothermal heating at 35 °C (Figure 12). Initially, the surface morphology was remarkably smooth. After approximately 90 minutes, the appearance of "pit" formations began to occur due to aniline's desolvation. As the crystal sample continued to undergo isothermal heating, these "pit" formations grew in size which led to greater surface roughening. Interestingly, the crystal showed signs of reconstruction into a different crystalline phase after approximately 600 minutes. The progression of the reconstruction occurred at a much faster rate than the previous pit formations.

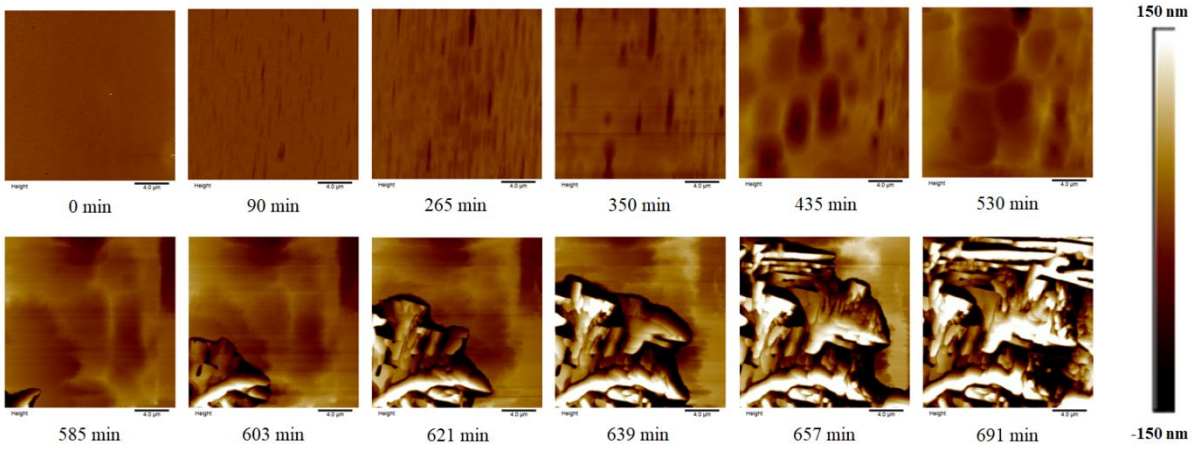

Figure 12. Evolution of AFM height images for the surface of a single TNT/aniline cocrystal solvate during isothermal heating at 35 °C. The top row shows growth of "pit" formations likely related to the desolvation of aniline. The bottom row shows an apparent reconstruction of the sample's surface into a different crystalline phase. All images are 20 μm ×20 μm^2.

3.5. Theoretical Explosive Parameters

In order to better understand the detonation properties of this new compound, theoretical calculations were performed to assess the safety and viability as an explosive. Theoretical values for the oxygen balance (*OB*), the packing coefficient (κ), the velocity of detonation (*VOD*), the detonation pressure (P_{cj}), and the heat of detonation (ΔH_{det}) for both pure TNT and a TNT/aniline cocrystal solvate are shown in Table 2. For the pure TNT crystal, all values can be readily determined via empirical calculations[25]. The packing coefficients were determined based on the work by Politzer[94,95]. The intrinsic volumes used in these calculations were determined from the group summation of the respective molecular volumes provided by Bondi[96]. Previous reports by Sherwood and co-workers indicate the crystal density of pure TNT to be 1.713 (at -173 °C) and 1.704 g cm^{-3} (at -150 °C) for the monoclinic and orthorhombic polymorphs, respectively[42]. The crystal density of the TNT/aniline cocrystal solvate reported here was found to be 1.550 g cm^{-3} (at -173 °C) using SCXRD (Table 1). For the cocrystal solvate, OB and κ were calculated by summing the total mass contribution due to the presence of aniline in 1:1 stoichiometric ratio with TNT. The theoretical values of the *VOD*, P_{cj}, and ΔH_{det} were determined via theoretical calculations performed using the computer code CHEETAH (ver. 8.0)[97–100].

Table 2. Comparison of theoretically calculated explosive parameters for a TNT/aniline cocrystal relative to pure TNT.

Sample Type	Oxygen Balance (OB) (%)	Packing Coefficient (κ)	Velocity of Detonation (VOD) (km s^{-1})	Detonation Pressure (P_{cj}) (GPa)	Enthalpy of Detonation (ΔH_{det}) (kJ g^{-1})
Explosive Parameters for Pure TNT	-74[a,c]	0.746[b]	7.21†; 7.00[a]; 6.85[c]	20.1†; 19[a]	4.46†; 3.72[a]; 4.48[c]
Theoretical Parameters for TNT/aniline	-130[a,*]	0.769[b,*]	6.50†	13.55†	3.64†

Cocrystal Solvate						

[a] From Ref.[25]; Note: For the general formula $C_aH_bN_cO_d$: $OB\ (\%) = \frac{d - 2a - \frac{b}{2}}{MW} * 1600$

[b] See ref.[95] for information on packing coefficient determination. The intrinsic volumes are based on the group contribution method where the explicit values were taken from ref.[96].

*Summation of individual group contributions for both aniline and TNT.

[c] From Ref.[90]

†Calculated using CHEETAH software version 8.0. The detonation velocity and pressure are computed at the Chapman-Jouguet (C-J) point.

4. Conclusion

TNT crystals grown from aniline resulted in the production of a cocrystal solvate with a vibrant red appearance. SCXRD measurements showed that TNT and aniline cocrystallized in a 1:1 stoichiometric ratio with an orthorhombic crystal lattice. The correctness and stability of atomic positions have been verified by first-principles DFT calculations, which show little deviation from the experimentally solved structure. Evidence obtained in several measurements indicate that cocrystallization of TNT and aniline occurs via formation of a charge-transfer complex. The mechanism of charge-transfer likely results from delocalization of aniline's lone electron pair on the amine group into the π-orbitals as shown in Figure 2. This is mostly supported in the crystal structure from the reduction in aniline's C–N bond length and the coplanar arrangement between opposite molecular pairs in which there is close-stacking between the respective phenyl rings. The most notable feature that indicates the formation of charge-transfer complex is the appearance of a broad absorbance band in the visible region (~495 nm).

Visual discoloration of the cocrystal solvate under ambient conditions suggests aniline desolvation occurs spontaneously. DSC, TG, IR, and PXRD measurements demonstrated that the cocrystal solvate recrystallizes into pure TNT upon desolvation. The PXRD measurements

indicated that there is a short-lived amorphous phase before fully recrystallizing into pure TNT crystals. The desolvation process was also monitored at the surface using *in situ* AFM measurements. The mechanism of crystal transformation due to desolvation has been suggested to occur via displacive motion[101–103] or a reconstructive phase transition[104,105.] Similar studies have used AFM to describe comparable solid-state transformations related to, for example, dehydration[106], polymorphic transitions[107,108], and amorphous crystallization[109,110]. However, the AFM results shown here are, to the best of our knowledge, the first to exhibit *in situ* recrystallization originating from internal desolvation.

Both the referenced and theoretically calculated results exhibited a general reduction in the explosive parameters for the TNT/aniline cocrystal solvate when compared to pure TNT. Specifically, the cocrystal solvate's *OB* (~76%), *VOD* (~8%), P_{cj} (~40%), ΔH_{det} (~2%), and density (~10%) were all found to be less than that of pure TNT. By definition, the packing coefficient is the fraction of the unit cell volume occupied by the given molecules[95] such that an increase in κ is expected based on the inverse relationship between the volume and density. The melting temperature was the only parameter found to result in an increase to that of pure TNT (~5 ^{o}C). Future investigations are warranted regarding *in situ* experimental measurements of the explosive parameters as well as the sensitivity.

ASSOCIATED CONTENT

Accession Codes

CCDC 1919306 contains the supplementary crystallographic data for this paper. These data can be obtained free of charge via www.ccdc.cam.ac.uk/data_request/cif, or by emailing data_request@ccdc.cam.ac.uk, or by contacting The Cambridge Crystallographic Data Centre, 12 Union Road, Cambridge CB2 1EZ, UK; fax: +44 1223 336033.

ASSOCIATED CONTENT

The Supporting Information is available free of charge on the ACS Publications website at:

Supporting Information A – Sections S1, S2, and S3

Section S1 – Additional Preparation Procedures for the Cocrystal Solvate

Figure S1. Example of solvent/antisolvent precipitation of a TNT/aniline solution in hexanes to yield the cocrystal solvate

Section S2 – UV/VIS Absorbance of Aniline; Experimental Method

Figure S2. UV/VIS absorbance spectrum of aniline.

Section S3 – Examples of Diffraction Pattern Baselines of the Cocrystal Solvate after 0.5 and 93 Hours Relative to the Orthorhombic Polymorph of Pure TNT

Figure S3. Close-up of the diffractogram baselines of the cocrystal solvate sample (blue) and the orthorhombic polymorph of pure TNT (black)

Supporting Information B – Section S4

Section S4. Summary of the Reitveld Analysis for the PXRD Measurements Related to the Desolvation of Aniline from the Cocrystal Solvate

AUTHOR INFORMATION

Corresponding Author

* E-mail: brandon.weeks@ttu.edu

Address**:** Texas Tech University Office of the Dean of Engineering Box 43103 Lubbock, TX 79409−3103

Author Contributions

The manuscript was written through contributions of all authors. All authors have given approval to the final version of the manuscript. The authors declare no competing financial interest.

[#]Nadia S. Fondren and Zachary T. Fondren contributed equally to this work.

ACKNOWLEDGMENT

The authors are grateful for financial support provided by the U.S. Department of Homeland Security under Award Number 2008-ST-061-ED0001. The views and conclusions expressed within this report are those of the authors and should not be interpreted as necessarily representing the official policies, either expressed or implied, of the U.S. Department of Homeland Security. Thanks also goes to the J.R. Bradford Endowment at Texas Tech University for partial financial support. Thanks to Dr. G.B. McKenna (Texas Tech University) for his encouragement and support throughout the editing and submission process. Thanks to Dr. Michael F. Meyer (Texas Tech University) for contributing his time towards discussing NMR data and charge-transfer complexes.

ABBREVIATIONS

TNT, 2,4,6-trinitrotoluene; PETN, pentaerythritol tetranitrate; HMX, 1,3,5,7-Tetranitro-1,3,5,7-tetrazoctane; RDX, cyclotrimethylenetrinitramine; CL-20, Hexanitrohexaazaisowurtzitane; FOX-7, 2,2-Dinitroethene-1,1-diamine; SCXRD and PXRD, single crystal and powder X-ray diffraction; DSC, differential scanning calorimetry; TG, thermogravimetry; HPLC, high performance liquid chromatography; AFM, atomic force microscopy; ATR-FTIR, attenuated

total reflection Fourier transform infrared spectroscopy; H/C NMR, hydrogen/carbon nuclear magnetic resonance; HOMO, highest occupied molecular orbital; LUMO, lowest occupied molecular orbital; OB, oxygen balance; VOD, velocity of detonation; P_{cj}, Chapman-Jouget detonation pressure

REFERENCES

(1) Landenberger, K. B.; Matzger, A. J. Cocrystals of 1,3,5,7-Tetranitro-1,3,5,7-Tetrazacyclooctane (HMX). *Cryst. Growth Des.* **2012**, *12*, 3603–3609, DOI: 10.1021/cg3004245

(2) Lara-Ochoa, F.; Espinosa-Pérez, G. Cocrystals Definitions. *Supramol. Chem.* **2007**, *19*, 553–557, DOI: 10.1080/10610270701501652

(3) Childs, S. L.; Zaworotko, M. J. The Reemergence of Cocrystals: The Crystal Clear Writing Is on the Wall Introduction to Virtual Special Issue on Pharmaceutical Cocrystals. *Cryst. Growth Des.* **2009**, *9*, 4208–4211, DOI: 10.1021/cg901002y

(4) Zhang, H.; Guo, C.; Wang, X.; Xu, J.; He, X.; Liu, Y.; Liu, X.; Huang, H.; Sun, J. Five Energetic Cocrystals of BTF by Intermolecular Hydrogen Bond and P-Stacking Interactions. *Cryst. Growth Des.* **2013**, *13*, 679–687, DOI: 10.1021/cg301353f

(5) Guo, C.; Zhang, H.; Wang, X.; Liu, X.; Sun, J. Study on a Novel Energetic Cocrystal of TNT/TNB. *J. Mater. Sci.* **2013**, *48*, 1351–1357, DOI: 10.1007/s10853-012-6881-5

(6) Horst, J. H. T.; Deij, M. A.; Cains, P. W. Discovering New Co-Crystals. *Cryst. Growth Des.* **2009**, *9*, 1531–1537, DOI: 10.1021/cg801200h

(7) Shan, N.; Zaworotko, M. J. The Role of Co-Crystals in Pharmaceutical Design. *Drug*

Discov. Today **2008**, *13*, 440–446, DOI: 10.1016/j.tips.2012.12.003

(8) Zaworotko, M. J. Molecules to Crystals, Crystals to Molecules... and Back Again? *Cryst. Growth Des.* **2007**, *7*, 4–9, DOI: 10.1021/cg0680172

(9) Desiraju, G. R. Counterpoint: What's in a Name? *Cryst. Growth Des.* **2004**, *4*, 1089–1090, DOI: 10.1021/cg030085q

(10) Yang, Z.; Li, H.; Huang, H.; Zhou, X.; Li, J.; Nie, F. Preparation and Performance of a HNIW/TNT Cocrystal Explosive. *Propellants, Explos. Pyrotech.* **2013**, *38*, 495–501, DOI: 10.1002/prep.201200093

(11) Landenberger, K. B.; Matzger, A. J. Cocrystal Engineering of a Prototype Energetic Material: Supramolecular Chemistry of 2,4,6-Trinitrotoluene. *Cryst. Growth Des.* **2010**, *10*, 5341–5347, DOI: 10.1021/cg101300n

(12) Bolton, O.; Simke, L. R.; Pagoria, P. F.; Matzger, A. J. High Power Explosive with Good Sensitivity: A 2:1 Cocrystal of CL-20:HMX. *Cryst. Growth Des.* **2012**, *12*, 4311–4314, DOI: 10.1021/cg3010882

(13) Oswald, I. D. H.; Motherwell, W. D. S.; Parsons, S. A 1:1 Co-Crystal of Quinol and Pyridine. *Acta Crystallogr. Sect. E Struct. Reports Online* **2004**, *60*, 1967–1969, DOI: 10.1107/S1600536804024547

(14) Shen, J. P.; Duan, X. H.; Luo, Q. P.; Zhou, Y.; Bao, Q.; Ma, Y. J.; Pei, C. H. Preparation and Characterization of a Novel Cocrystal Explosive. *Cryst. Growth Des.* **2011**, *11*, 1759–1765, DOI: 10.1039/c3dt51594j

(15) Dunitz, J. D. Crystal and Co-Crystal: A Second Opinion. *CrystEngComm* **2003**, *5*, 506,

DOI: 10.1039/b315687g

(16) Jetti, R. K. R.; Boese, R.; Thallapally, P. K.; Desiraju, G. R. Five New Pseudopolymorphs of Sym-Trinitrobenzene. *Cryst. Growth Des.* **2003**, *3*, 1033–1040, DOI: 10.1021/cg034141z

(17) Seddon, K. R. Pseudo Polymorph: A Polemic. *Cryst. Growth Des.* **2004**, *4*, 1087–1087, DOI: 10.1021/cg030084y

(18) Bernstein, J. ....And Another Comment on Pseudo Polymorphism. *Cryst. Growth Des.* **2005**, *5*, 1661–1662, DOI: 10.1021/cg058007l

(19) Nangia, A. Pseudopolymorph: Retain This Widely Accepted Term. *Cryst. Growth Des.* **2006**, *6*, 2–4, DOI: 10.1021/jm060379l

(20) Vishweshwar, P.; McMahon, J. A.; Bis, J. A.; Zaworotko, M. J. Pharmaceutical Co-Crystals. *J. Pharm. Sci.* **2006**, *95*, 499–516, DOI: 10.1002/jps.20578

(21) Blagden, N.; de Matas, M.; Gavan, P. T.; York, P. Crystal Engineering of Active Pharmaceutical Ingredients to Improve Solubility and Dissolution Rates. *Adv. Drug Deliv. Rev.* **2007**, *59*, 617–630, DOI: 10.1016/j.addr.2007.05.011

(22) Qiao, N.; Li, M.; Schlindwein, W.; Malek, N.; Davies, A.; Trappitt, G. Pharmaceutical Cocrystals: An Overview. *Int. J. Pharm.* **2011**, *419*, 1–11, DOI: 10.1016/j.ijpharm.2011.07.037

(23) Stahly, G. P. Diversity in Single- and Multiple-Component Crystals. The Search for and Prevalence of Polymorphs and Cocrystals. *Cryst. Growth Des.* **2007**, *7*, 1007–1026, DOI: 10.1021/cg060838j

(24) Grothe, E.; Meekes, H.; Vlieg, E.; Ter Horst, J. H.; De Gelder, R. Solvates, Salts, and Cocrystals: A Proposal for a Feasible Classification System. *Cryst. Growth Des.* **2016**, *16*, 3237–3243, DOI: 10.1021/acs.cgd.6b00200

(25) Agrawal, J. P. *High Energy Materials: Propellants, Explosives, and Pyrotechnics*; Wiley-VCH Verlag GmbH & Co. KGaA: Weinheim, Germany, 2010

(26) Nielsen, A. T.; Chafin, A. P.; Christian, S. L.; Moore, D. W.; Nadler, M. P.; Nissan, R. A.; Vanderah, D. J.; Gilardi, R. D.; George, C. F.; Flippen-Anderson, J. L. Synthesis of Polyazapolycyclic Caged Polynitramines. *Tetrahedron* **1998**, *54*, 11793–11812, DOI: 10.1016/S0040-4020(98)83040-8

(27) Bemm, U.; Östmark, H. 1,1-Diamino-2,2-Dinitroethylene: A Novel Energetic Material with Infinite Layers in Two Dimensions. *Acta Crystallogr. Sect. C Cryst. Struct. Commun.* **1998**, *54*, 1997–1999, DOI: 10.1107/S0108270198007987

(28) Gong, F.; Zhang, J.; Ding, L.; Yang, Z.; Liu, X. Mussel-Inspired Coating of Energetic Crystals: A Compact Core-Shell Structure with Highly Enhanced Thermal Stability. *Chem. Eng. J.* **2017**, *309*, 140–150, DOI: 10.1016/j.cej.2016.10.020

(29) Stepanov, V.; Patel, R. B.; Mudryy, R.; Qiu, H. Investigation of Nitramine-Based Amorphous Energetics. *Propellants, Explos. Pyrotech.* **2016**, *41*, 142–147, DOI: 10.1002/prep.201500118

(30) Li, J.; Brill, T. B. Kinetics of Solid Polymorphic Phase Transitions of CL-20. *Propellants, Explos. Pyrotech.* **2007**, *32*, 326–330, DOI: 10.1002/prep.200700036

(31) Goldberg, I. G.; Swift, J. A. New Insights into the Metastable β Form of RDX. *Cryst.*

Growth Des. **2012**, *12*, 1040–1045, DOI: 10.1021/cg201718a

(32) Karimi-Jafari, M.; Padrela, L.; Walker, G. M.; Croker, D. M. Creating Cocrystals: A Review of Pharmaceutical Cocrystal Preparation Routes and Applications. *Cryst. Growth Des.* **2018**, *18*, 6370–6387, DOI: 10.1021/acs.cgd.8b00933

(33) Qiu, H.; Patel, R. B.; Damavarapu, R. S.; Stepanov, V. Nanoscale 2CL-20·HMX High Explosive Cocrystal by Bead Milling. *CrystalEngComm* **2015**, *17*, 4080–4083, DOI: 10.1039/C5CE00489F

(34) Shi, L.; Duan, X. H.; Zhu, L. G.; Liu, X.; Pei, C. H. Directly Insight into the Inter- and Intramolecular Interactions of CL-20/TNT Energetic Cocrystal through the Theoretical Simulations of THz Spectroscopy. *J. Phys. Chem. A* **2016**, *120*, 1160–1167, DOI: 10.1021/acs.jpca.5b10782

(35) An, C.; Li, H.; Ye, B.; Wang, J. Nano-CL-20/HMX Cocrystal Explosive for Significantly Reduced Mechanical Sensitivity. *J. Nanomater.* **2017**, *2017*, DOI: 10.1155/2017/3791320

(36) Millar, D. I. A.; Maynard-Casely, H. E.; Allan, D. R.; Cumming, A. S.; Lennie, A. R.; Mackay, A. J.; Oswald, I. D. H.; Tang, C. C.; Pulham, C. R. Crystal Engineering of Energetic Materials: Co-Crystals of CL-20. *CrystEngComm* **2012**, *14*, 3742–3749, DOI: 10.1039/c2ce05796d

(37) Yang, Z.; Li, H.; Zhou, X.; Zhang, C.; Huang, H.; Li, J.; Nie, F. Characterization and Properties of a Novel Energetic-Energetic Cocrystal Explosive Composed of HNIW and BTF. *Cryst. Growth Des.* **2012**, *12*, 5155–5158, DOI: 10.1021/cg300955q

(38) Gao, B.; Wang, D.; Zhang, J.; Hu, Y.; Shen, J.; Wang, J.; Huang, B.; Qiao, Z.; Huang, H.;

Nie, F.; et al. Facile, Continuous and Large-Scale Synthesis of CL-20/HMX Nano Co-Crystals with High-Performance by Ultrasonic Spray-Assisted Electrostatic Adsorption Method. *J. Mater. Chem. A* **2012**, *2*, 19969–19974, DOI: 10.1039/C4TA04979A

(39) Li, H.; An, C.; Guo, W.; Geng, X.; Wang, J.; Xu, W. Preparation and Performance of Nano HMX/TNT Cocrystals. *Propellants, Explos. Pyrotech.* **2015**, *40*, 652–658, DOI: 10.1002/prep.201400175

(40) Hong, D.; Li, Y.; Zhu, S.; Zhang, L.; Pang, C. Three Insensitive Energetic Co-Crystals of 1-Nitronaphthalene, with 2,4,6-Trinitrotoluene (TNT), 2,4,6-Trinitrophenol (Picric Acid) and D-Mannitol Hexanitrate (MHN). *Cent. Eur. J. Energ. Mater.* **2015**, *12*, 47–62

(41) Gallagher, H. G.; Sherwood, J. N. Polymorphism, Twinning and Morphology of Crystals of 2,4,6-Trinitrotoluene Grown from Solution. *J. Chem. Soc. Faraday Trans.* **1996**, *92*, 2107–2116, DOI: 10.1039/FT9969202107

(42) Vrcelj, R. M.; Sherwood, J. N.; Kennedy, A. R.; Gallagher, H. G.; Gelbrich, T. Polymorphism in 2-4-6 Trinitrotoluene. *Cryst. Growth Des.* **2003**, *3*, 1027–1032, DOI: 10.1021/cg0340704

(43) Vrcelj, R. M.; Gallagher, H. G.; Sherwood, J. N. Polymorphism in 2,4,6-Trinitrotoluene Crystallized from Solution. *J. Am. Chem. Soc.* **2001**, *123*, 2291–2295, DOI: 10.1021/ja0031422

(44) Fondren, S. N.; Fondren, Z. T.; Unruh, D. K.; Weeks, B. L. Unpublished Work. Texas Tech University. **2019**

(45) Fant, F.; De Sloovere, A.; Matthijsen, K.; Marle, C.; El Fantroussi, S.; Verstraete, W. The

Use of Amino Compounds for Binding 2,4,6-Trinitrotoluene in Water. *Environ. Pollut.* **2001**, *111*, 503–507, DOI: 10.1016/S0269-7491(00)00077-4

(46) Gao, D.; Wang, Z.; Liu, B.; Ni, L.; Wu, M.; Zhang, Z. Resonance Energy Transfer-Amplifying Fluorescence Quenching at the Surface of Silica Nanoparticles toward Ultrasensitive Detection of TNT. *Anal. Chem.* **2008**, *80*, 8545–8553, DOI: 10.1021/ac8014356

(47) Tu, R.; Liu, B.; Wang, Z.; Gao, D.; Wang, F.; Fang, Q.; Zhang, Z.; Zns, M. Amine-Capped ZnS−Mn2+ Nanocrystals for Fluorescence Detection of Trace TNT Explosive. *Anal. Chem.* **2008**, *80*, 3458–3465, DOI: 10.1021/ac800060f

(48) Dasary, S. S. R.; Singh, A. K.; Senapati, D.; Yu, H.; Ray, P. C. Gold Nanoparticle Based Label-Free SERS Probe for Ultrasensitive and Selective Detection of Trinitrotoluene. *J. Am. Chem. Soc.* **2009**, *131*, 13806–13812, DOI: 10.1021/ja905134d

(49) Liu, Y.; Wang, H. H.; Indacochea, J. E.; Wang, M. L. A Colorimetric Sensor Based on Anodized Aluminum Oxide (AAO) Substrate for the Detection of Nitroaromatics. *Sensors Actuators, B Chem.* **2011**, *160*, 1149–1158, DOI: 10.1016/j.snb.2011.09.040

(50) Zhang, K.; Zhou, H.; Mei, Q.; Wang, S.; Guan, G.; Liu, R.; Zhang, J.; Zhang, Z. Instant Visual Detection of Trinitrotoluene Particulates on Various Hybrid. *J. Am. Chem. Soc.* **2011**, *133*, 8424–8427, DOI: 10.1021/ja2015873

(51) Hughes, S.; Dasary, S. S. R.; Begum, S.; Williams, N.; Yu, H. Meisenheimer Complex between 2,4,6-Trinitrotoluene and 3-Aminopropyltriethoxysilane and Its Use for a Paper-Based Sensor. *Sens. Bio-Sensing Res.* **2015**, *5*, 37–41, DOI: 10.1016/j.sbsr.2015.06.003

(52) Ueda, H.; Sakabe, N.; Tanaka, J.; Furusaki, A. The Structure of Meisenheimer Crystal Complex Analysis as Determined by X-Ray Crystal Analysis. *Bull. Chem. Soc. Jpn.* **1968**, *41*, 2866–2871, DOI: 10.1246/bcsj.41.2866

(53) Bacaloglu, R.; Bunton, C. A.; Ortega, F. Single-Electron Transfer in Aromatic Nucleophilic Addition and Substitution in Aqueous Media. *J. Am. Chem. Soc.* **1988**, *110*, 3503–3512, DOI: 10.1021/ja00219a026

(54) Mulliken, R. S. Molecular Compounds and Their Spectra. II. *J. Am. Chem. Soc.* **1952**, *74*, 811–824, DOI: 10.1021/ja01123a067

(55) Mulliken, R. S. Molecular Compounds and Their Spectra. III. The Interaction of Electron Donors and Acceptors. *J. Phys. Chem.* **1952**, *56*, 801–822, DOI: 10.1021/j150499a001

(56) Mulliken, R. S. The Interaction of Electron Donors and Acceptors. *J. Chim. Phys.* **1964**, *61*, 20–39, DOI: 10.1051/jcp/1964610020

(57) Andrews, L. J.; Keefer, R. M. *Molecular Complexes in Organic Chemistry*; Holden-Day, Inc., 1964

(58) Rose, J. *Molecular Complexes*, 1st Ed.; Pergamon Press Ltd., 1967

(59) Foster, R. *Organic Charge-Transfer Complexes*; Blomquist, A. T., Ed.; Academic Press, Inc. (London) Ltd., 1969

(60) Landaubr, J.; McConnell, H. A Study of Molecular Complexes Formed by Aniline and Aromatic Nitrohydrocarbons. *J. Am. Chem. Soc.* **1952**, *74*, 1221–1224, DOI: 10.1021/ja01125a025

(61) Ross, S. D.; Labes, M. M. Molecular Compounds. V. Solvent Effects on Complexing of 1, 3, 5-Trinitrobenzene with Aniline and with Naphthalene. *J. Am. Chem. Soc.* **1955**, *77*, 4916–4920, DOI: 10.1021/ja01623a069

(62) Liptay, V. W.; Briegleb, G.; Schindler, K. Elektronen-Donator-Akzeptor-Komplex- Und Ionenbildung Bei Der Wechsel- Wirkung von N, N, N', N'-Tetramethyl-p-Phenylendiamin Mit Tetracyanathylen. *Zeitschrift für Elektrochemie* **1962**, *66*, 331–341

(63) Foster, R.; Fyfe, C. A. Interaction of Electron Acceptors with Bases. Part 15.—Determination of Association Constants of Organic Charge-Transfer Complexes by Nmr Spectroscopy. *Trans. Faraday Soc.* **1965**, *61*, 1626–1631, DOI: 10.1039/TF9656101626

(64) Foster, R.; Fyfe, C. Y. Interaction of Electron Acceptors with Bases-XIX. The Interaction of 1,3,5-Trinitrobenzene with Secondory Amines in Acetone Solution. *Tetrahedron* **1967**, *23*, 528, DOI: 10.1016/S0040-4020(01)83340-8

(65) Buncel, E.; Webb, J. G. K. An Aromatic Amine- 1,3,5-Trinitrobenzene σ-Complex. *Can. J. Chem.* **1972**, *50*, 129–131, DOI: 10.1139/v72-021

(66) Lichtfus, G.; Zeegers-Huyskens, T. Vibrational Spectra of Some Charge-Transfer Complexes of Anilines. *Bull. des Sociétés Chim. Belges* **1973**, *82*, 123–131, DOI: 10.1002/bscb.19730820110

(67) Park, S.; Herndon, W. C. Determination of Dimerization Constants of Organic Compounds by Nmr Spectrometric Methods. *Tetrahedron Lett.* **1978**, *19*, 2363–2366, DOI: 10.1016/S0040-4039(01)94775-6

(68) Abdulla, R. F.; Boyd, D. B.; Jones, N. D.; Swartzendruber, J. K. Evidence for an Unusual

Charge-Transfer Complex in (Nitrophenacyl) Anilines. *J. Org. Chem.* **1985**, *50*, 3502–3505, DOI: 10.1021/jo00219a016

(69) Taylor, C. A.; Rinkenbach, W. H. The Solubility of Trinitrotoluene in Organic Solvents. *J. Am. Chem. Soc.* **1923**, *45*, 44–59, DOI: 10.1021/ja01654a006

(70) Krause, L.; Herbst-Irmer, R.; Sheldrick, G. M.; Stalke, D. Comparison of Silver and Molybdenum Microfocus X-Ray Sources for Single-Crystal Structure Determination. *J. Appl. Crystallogr.* **2015**, *48*, 3–10, DOI: 10.1107/S1600576714022985

(71) Sheldrick, G. M. A Short History of SHELX. *Acta Crystallogr. Sect. A Found. Crystallogr.* **2007**, *64*, 112–122, DOI: 10.1107/S0108767307043930

(72) Zhu, W.; Zheng, R.; Fu, X.; Fu, H.; Shi, Q.; Zhen, Y.; Dong, H.; Hu, W. Revealing the Charge-Transfer Interactions in Self-Assembled Organic Cocrystals: Two-Dimensional Photonic Applications. *Angew. Chemie - Int. Ed.* **2015**, *54*, 6785–6789, DOI: 10.1002/anie.201501414

(73) Hu, P.; Du, K.; Wei, F.; Jiang, H.; Kloc, C. Crystal Growth, HOMO-LUMO Engineering, and Charge Transfer Degree in Perylene-F_xTCNQ (x = 1, 2, 4) Organic Charge Transfer Binary Compounds. *Cryst. Growth Des.* **2016**, *16*, 3019–3027, DOI: 10.1021/acs.cgd.5b01675

(74) Santra, D. C.; Bera, M. K.; Sukul, P. K.; Malik, S. Charge-Transfer-Induced Fluorescence Quenching of Anthracene Derivatives and Selective Detection of Picric Acid. *Chem. - A Eur. J.* **2016**, *22*, 2012–2019, DOI: 10.1002/chem.201504126

(75) Sun, Y.; Lei, Y.; Liao, L.; Hu, W. Competition between Arene–Perfluoroarene and Charge-

Transfer Interactions in Organic Light-Harvesting Systems. *Angew. Chemie - Int. Ed.* **2017**, *56*, 10352–10356, DOI: 10.1002/anie.201702084

(76) Lister, D. G.; Tyler, J. K.; Høg, J. H.; Larsen, N. W. The Microwave Spectrum, Structure and Dipole Moment of Aniline. *J. Mol. Struct.* **1974**, *23*, 253–264, DOI: 10.1016/0022-2860(74)85039-8

(77) Niu, Z.; Boggs, J. E. The Structure of Aniline. *J. Mol. Struct.* **1984**, *109*, 381–389, DOI: 10.1016/0166-1280(84)80022-6

(78) Wojciechowski, P. M.; Zierkiewicz, W.; Michalska, D.; Hobza, P. Electronic Structures, Vibrational Spectra, and Revised Assignment of Aniline and Its Radical Cation: Theoretical Study. *J. Chem. Phys.* **2003**, *18*, 10900–10911, DOI: 10.1063/1.1574788

(79) Delley, B. From Molecules to Solids with the DMol^3 Approach. *J. Chem. Phys.* **2000**, *113*, 7756–7764, DOI: 10.1063/1.1316015

(80) Perdew, J. P.; Burke, K.; Ernzerhof, M. Generalized Gradient Approximation Made Simple. *Phys. Rev. Lett.* **1996**, *77*, 3865–3868, DOI: 10.1103/PhysRevLett.77.3865

(81) Pack, J. D.; Monkhorst, H. J. Special Points for Brillouin-Zone Integrations. *Phys. Rev. B* **1976**, *13*, 5188–5192, DOI: 10.1103/PhysRevB.16.1748

(82) Meyer, R.; Köhler, J.; Homburg, A. *Explosives*, 5th Ed.; Wiley-VCH, 2002

(83) Rady, A. H. Spectroscopic Investigation on the Charge-Transfer Complex of 2, 4, 6-Trinitrophenol with the Polycyclicamine 1, 4, 8, 11-Tetraazacyclotetradecane. *Spectrosc. Lett.* **1992**, *25*, 327–338, DOI: 10.1080/00387019208018191

(84) Wu, H.; Du, L. M. Spectrophotometric Determination of Anilines Based on Charge-Transfer Reaction. *Spectrochim. Acta Part A Mol. Biomol. Spectrosc.* **2007**, *67*, 976–979, DOI: 10.1016/j.saa.2006.09.016

(85) Lei, Y. L.; Jin, Y.; Zhou, D. Y.; Gu, W.; Shi, X. B.; Liao, L. S.; Lee, S. T. White-Light Emitting Microtubes of Mixed Organic Charge-Transfer Complexes. *Adv. Mater.* **2012**, *24*, 5345–5351, DOI: 10.1002/adma.201201493

(86) Stewart, J. J. P.; Bosco, S. R.; Carper, W. R. Vibrational Spectra of 2,4,6-Trinitrotoluene and Its Isotopically Substituted Analogues. *Spectrochim. Acta Part A Mol. Spectrosc.* **1986**, *42*, 13–21, DOI: 10.1016/0584-8539(86)80124-6

(87) Evans, J. C. The Vibrational Assignments and Configuration of Aniline, Aniline-NHD and Aniline-ND_2. *Spectrochim. Acta* **1960**, *16*, 428–442, DOI: 10.1016/0371-1951(60)80037-9

(88) Piest, H.; Helden, G. Von; Meijer, G. Infrared Spectroscopy of Jet-Cooled Neutral and Ionized Aniline–Ar. *J. Chem. Phys.* **1999**, *110*, 2010–2014, DOI: 10.1063/1.477866

(89) Conley, R. T. *Infrared Spectroscopy*, 2nd ed.; Allyn and Bacon, Inc.: Boston, MA, 1972

(90) Akhavan, J. *The Chemistry of Explosives*; The Royal Soceity of Chemistry, 1998, DOI: 10.1007/BF02467569

(91) Dacons, J. C.; Kamlet, M. J.; Sickman, D. V. Thermal Decomposition of TNT. *Nav. ORDNANCE LAB WHITE OAK, MD* **1960**

(92) Gupta, S. K.; Nanotl, S. M.; Rawat, B. S. Vapor–Liquid Equilibria for the Systems Hexane–Aniline and Hexane–Benzene–Aniline at Atmospheric Pressure. *J. Chem. Eng. Data* **1992**, *37*, 162–164, DOI: 10.1021/je00006a006

(93) Lisac, K.; Nemec, V.; Topić, F.; Arhangelskis, M.; Hindle, P.; Tran, R.; Huskić, I.; Morris, A. J.; Friščić, T.; Cinčić, D. Experimental and Theoretical Investigation of Structures, Stoichiometric Diversity, and Bench Stability of Cocrystals with a Volatile Halogen Bond Donor. *Cryst. Growth Des.* **2018**, *18*, 2387–2396, DOI: 10.1021/acs.cgd.7b01808

(94) Politzer, P.; Murray, J. S.; Clark, T. Mathematical Modeling and Physical Reality in Noncovalent Interactions. *J. Mol. Model.* **2015**, *21*, DOI: 10.1007/s00894-015-2585-5

(95) Politzer, P.; Murray, J. S. Perspectives on the Crystal Densities and Packing Coefficients of Explosive Compounds. *Struct. Chem.* **2016**, *27*, 401–408, DOI: 10.1007/s11224-015-0702-9

(96) Bondi, A. Van Der Waals Volumes and Radii. *J. Phys. Chem.* **1964**, *68*, 441–451, DOI: 10.1021/j100785a001

(97) Keshavarz, M. H.; Motamedoshariati, H.; Moghayadnia, R.; Nazari, H. R.; Azarniamehraban, J. A New Computer Code to Evaluate Detonation Performance of High Explosives and Their Thermochemical Properties, Part I. *J. Hazard. Mater.* **2009**, *172*, 1218–1228, DOI: 10.1016/j.jhazmat.2009.07.128

(98) Keshavarz, M. H. Simple Procedure for Determining Heats of Detonation. *Thermochim. Acta* **2005**, *428*, 95–99, DOI: 10.1016/j.tca.2004.10.005

(99) Keshavarz, M. H.; Pouretedal, H. R. Predicting the Detonation Velocity of CHNO Explosives by a Simple Method. *Propellants, Explos. Pyrotech.* **2005**, *30*, 105–108, DOI: 10.1002/prep.200400091

(100) Keshavarz, M. H.; Pouretedal, H. R. An Empirical Method for Predicting Detonation

Pressure of CHNOFCl Explosives. *Thermochim. Acta* **2004**, *414*, 203–208, DOI: 10.1016/j.tca.2003.11.019

(101) Nicolai, B.; Espeau, P.; Céolin, R.; Perrin, M.; Zaske, L.; Giovannini, J.; Leveiller, F. POLYMORPH FORMATION FROM SOLVATE DESOLVATION Spironolactone Forms I and II from the Spironolactone-Ethanol Solvate. *J. Therm. Anal. Calorim.* **2007**, *90*, 337–339, DOI: 10.1007/s10973-007-8389-9

(102) Thakuria, R.; Eddleston, M. D.; Chow, E. H. H.; Lloyd, G. O.; Aldous, B. J.; Krzyzaniak, J. F.; Bond, A. D.; Jones, W. Use of In Situ Atomic Force Microscopy to Follow Phase Changes at Crystal Surfaces in Real Time. *Angew. Chemie Int. Ed.* **2013**, *52*, 10541–10544, DOI: 10.1002/anie.201302532

(103) Mehlana, G.; Ramon, G.; Bourne, S. A. The Role of C-H···π Interactions in Modulating the Breathing Amplitude of a 2D Square Lattice Net: Alcohol Sorption Studies. *CrystEngComm* **2014**, *16*, 8160–8168, DOI: 10.1039/c4ce00496e

(104) Matvienko, A. A.; Maslennikov, D. V.; Zakharov, B. A.; Sidelnikov, A. A.; Chizhik, S. A.; Boldyreva, E. V. Structural Aspects of Displacive Transformations: What Can Optical Microscopy Contribute? Dehydration of $Sm_2(C_2O_4)$ $3{\cdot}10H_2O$ as a Case Study. *IUCrJ* **2017**, *4*, 588–597, DOI: 10.1107/s2052252517008624

(105) Martins, D.; Sanselme, M.; Houssin, O.; Dupray, V.; Petit, M. N.; Pasquier, D.; Diolez, C.; Coquerel, G. Physical Transformations of the Active Pharmaceutical Ingredient BN83495: Enantiotropic and Monotropic Relationships. Access to Several Polymorphic Forms by Using Various Solvation-Desolvation Processes. *CrystEngComm* **2012**, *14*, 2507–2519, DOI: 10.1039/c2ce06537a

(106) Yuan, L.; Horosanskaia, E.; Engelhardt, F.; Edelmann, F. T.; Couvrat, N.; Seidel-morgenstern, A.; Sanselme, M.; Cartigny, Y. Solvate Formation of Bis(Demethoxy)Curcumin: Crystal Structure Analyses and Stability Investigations. *Cryst. Growth Des.* **2019**, *19*, 854–867, DOI: 10.1021/acs.cgd.8b01425

(107) Jones, M. D.; Beezer, A. E.; Buckton, G. Determination of Outer Layer and Bulk Dehydration Kinetics of Trehalose Dihydrate Using Atomic Force Microscopy, Gravimetric Vapour Sorption and Near Infrared Spectroscopy. *J. Pharm. Sci.* **2008**, *97*, 4404–4415, DOI: 10.1002/jps.21318

(108) Matsuo, K.; Matsuoka, M. Kinetics of Solid State Polymorphic Transition of Caffeine. *J. Chem. Eng. Japan* **2007**, *40*, 468–472, DOI: 10.1252/jcej.40.468

(109) Mahlin, D.; Berggren, J.; Alderborn, G.; Engström, S. Moisture-Induced Surface Crystallization of Spray-Dried Amorphous Lactose Particles Studied by Atomic Force Microscopy. *J. Pharm. Sci.* **2004**, *93*, 29–37, DOI: 10.1002/jps.10503

(110) Mahlin, D.; Berggren, J.; Gelius, U.; Engström, S.; Alderborn, G. The Influence of PVP Incorporation on Moisture-Induced Surface Crystallization of Amorphous Spray-Dried Lactose Particles. *Int. J. Pharm.* **2006**, *321*, 78–85, DOI: 10.1016/j.ijpharm.2006.05.016

For Table of Contents Use Only

Manuscript title

Study of Physicochemical and Explosive Properties of a 2,4,6-Trinitrotoluene/Aniline Cocrystal Solvate

Author List

Nadia S. Fondren, Zachary T. Fondren, Yong Joon Lee, Amitesh Maiti, Daniel K. Unruh, Louisa Hope-Weeks, Anthony Cozzolino and Brandon L. Weeks

Table of Contents Graphic

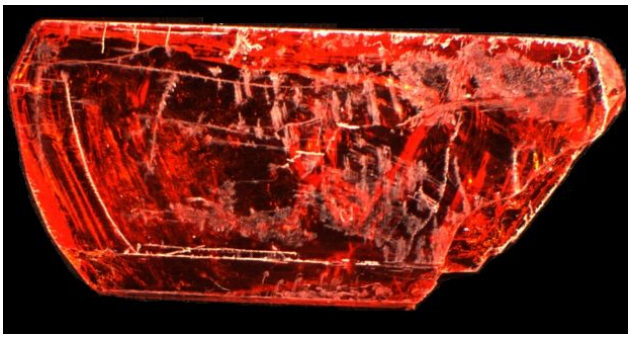

SYNOPSIS

2,4,6-Trinitrotoluene (TNT) was cocrystallized with aniline to produce a novel cocrystal solvate with a ruby red appearance in which experimental evidence suggests the mechanism is related to the formation of a charge-transfer complex. The lattice structure was determined with single-crystal X-ray diffraction and revealed the individual components to have a 1:1 molecular packing arrangement with an orthorhombic configuration. Phase change data was measured with differential scanning calorimetry (DSC). Evidence of aniline desolvation was experimentally observed and discussed. Theoretical calculations of the explosive parameters are also presented.

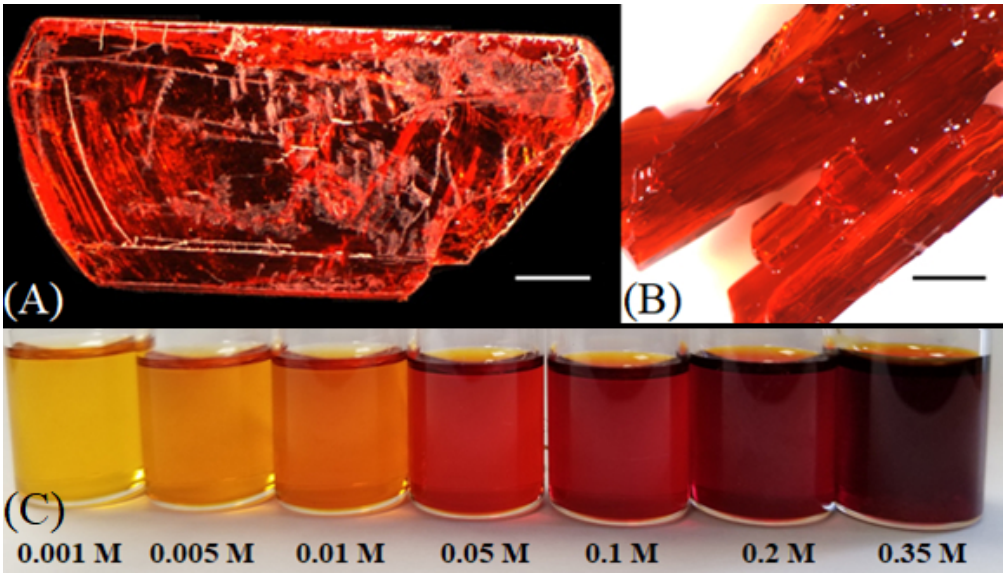

Figure 1. Macroscopic images of TNT/aniline cocrystal solvates grown with excess aniline at (A) room temperature (A) and 5 oC (B). The scale bar is approximately 2 mm. (C) Comparison of the progressive deepening in red color that occurs almost instantly within aniline solutions containing increasing concentrations of TNT.

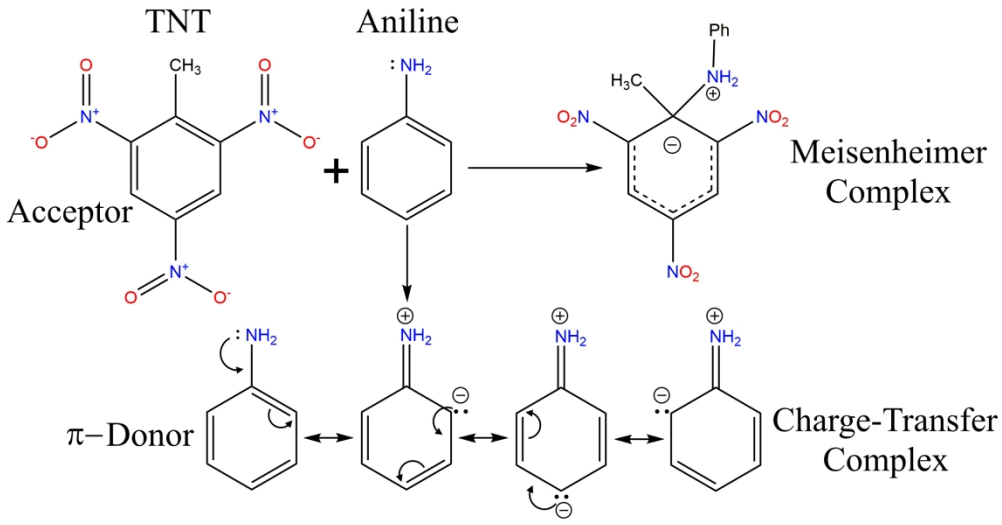

Figure 2. Comparison of the potential mechanisms in which TNT and aniline interact to produce the red color observed in the cocrystal solvate.

205x107mm (300 x 300 DPI)

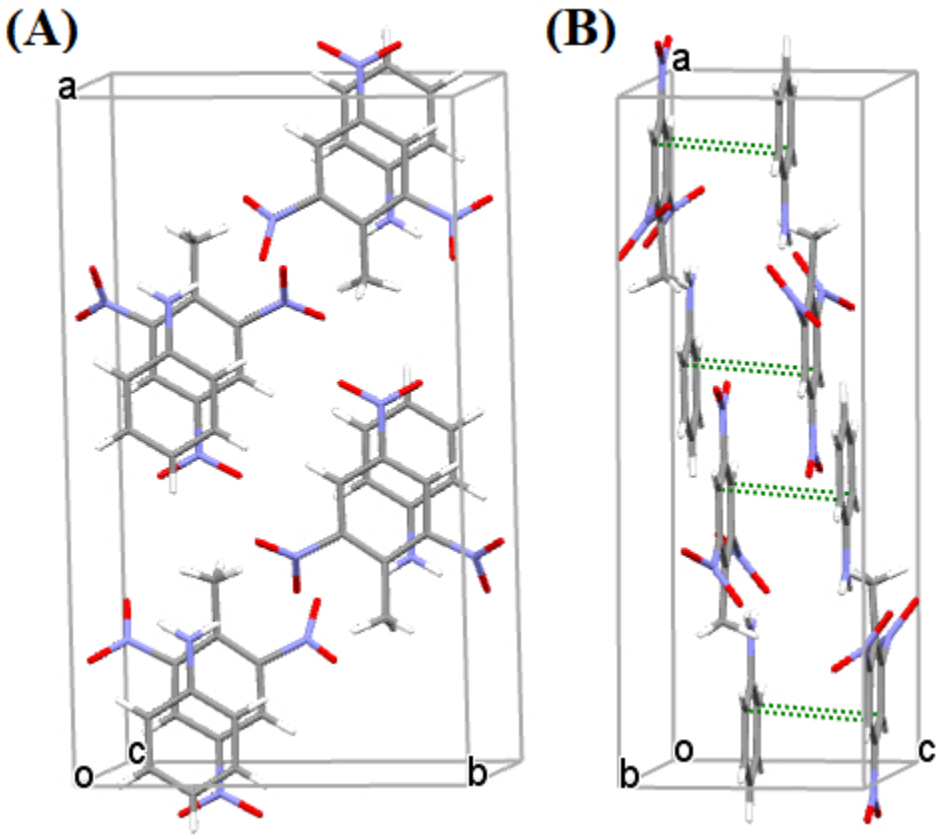

Figure 3. SCXRD representation of the packing arrangement and orientation of TNT and aniline present within the cocrystal solvate as viewed along the c-axis (A) and b-axis (B). The green dashed lines in (B) indicate intermolecular distances that are less than the sum of the Van der Waal radii. The depictions were created using the CCDC's Mercury software ver. 4.1.3. (Note: carbon – grey; nitrogen – blue; oxygen – red; hydrogen – white)

128x112mm (96 x 96 DPI)

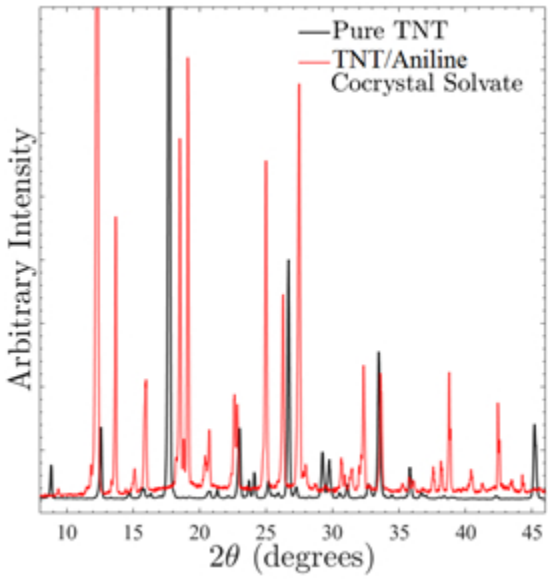

Figure 4. PXRD patterns for an orthorhombic crystal of pure TNT (black) and a TNT/aniline cocrystal solvate (red).

71x76mm (96 x 96 DPI)

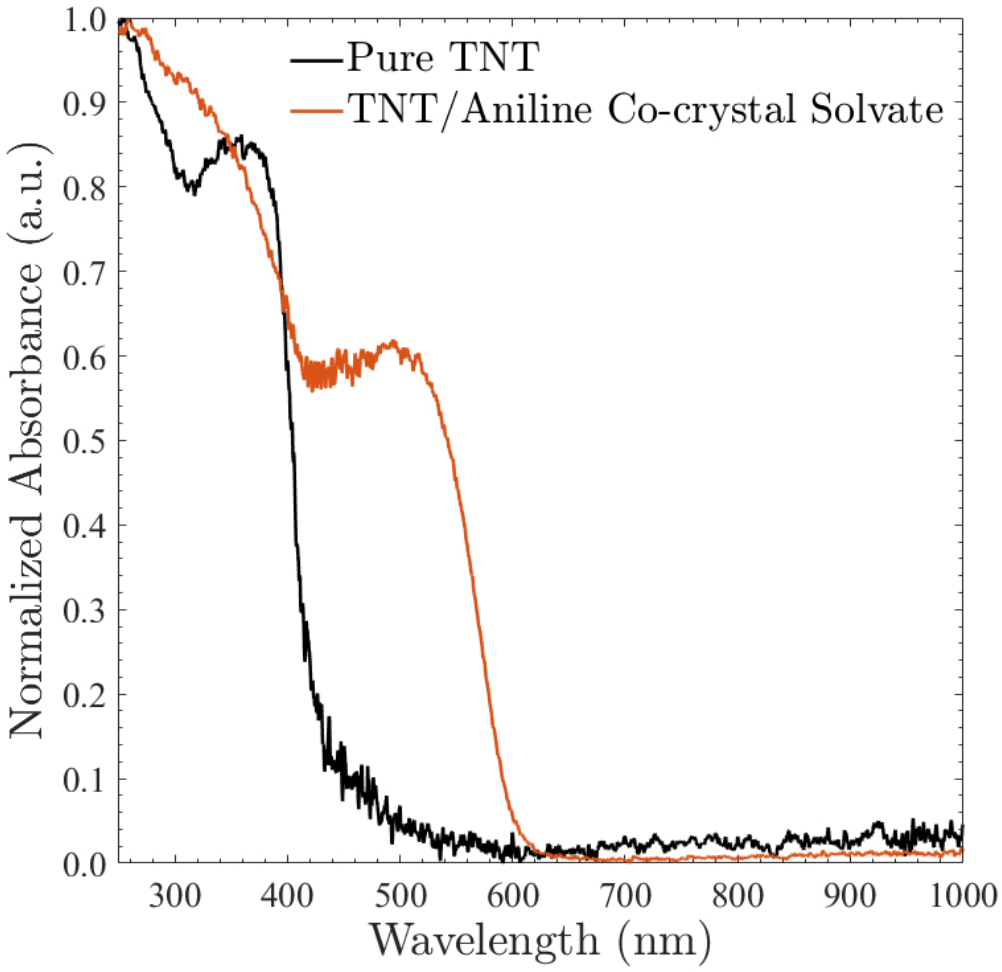

Figure 5. Diffuse reflectance absorbance spectra of pure TNT (black) and a TNT/aniline cocrystal solvate (red). The onset of spectral absorbance is redshifted in the cocrystal solvate (e.g. ~450 → ~600 nm) and exhibits a new peak whose maximum absorbance is around 495 nm. This result is consistent with the formation of a charge-transfer complex between TNT and aniline.

200x194mm (96 x 96 DPI)

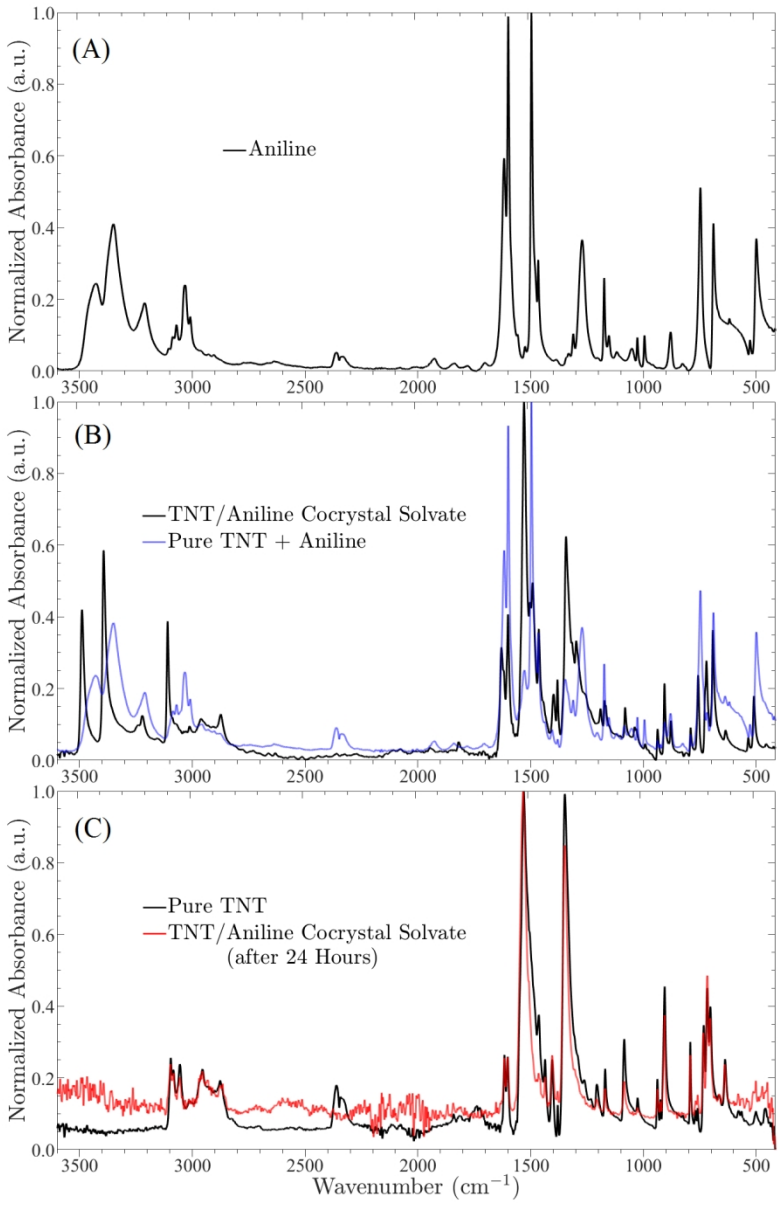

Figure 6. ATR-FTIR transmittance spectra of liquid aniline (A), a freshly prepared TNT/aniline cocrystal solvate (B), and a pure TNT crystal produced from toluene via antisolvent precipitation with water (C). A superposition of the TNT and aniline absorbances shown, respectively, in (A) and (C) are overlaid (blue) onto the cocrystal solvate spectra in (B), and the spectrum of a cocrystal solvate sample after exposure to air for 24 hours (i.e. complete discoloration from red to yellow) is overlaid (red) onto the pure TNT spectrum in (C). Note: The peaks at ~2350 cm-1 occur due to atmospheric carbon dioxide.

355x546mm (96 x 96 DPI)

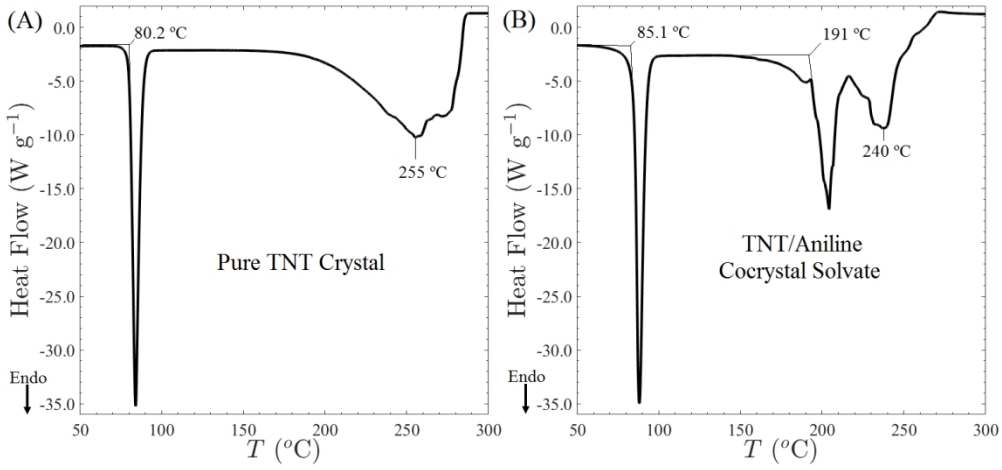

Figure 7. Experimental DSC traces of a pure TNT crystal (A) and a TNT/aniline cocrystal solvate (B) using a heating rate of 20 oC min-1.

414x192mm (96 x 96 DPI)

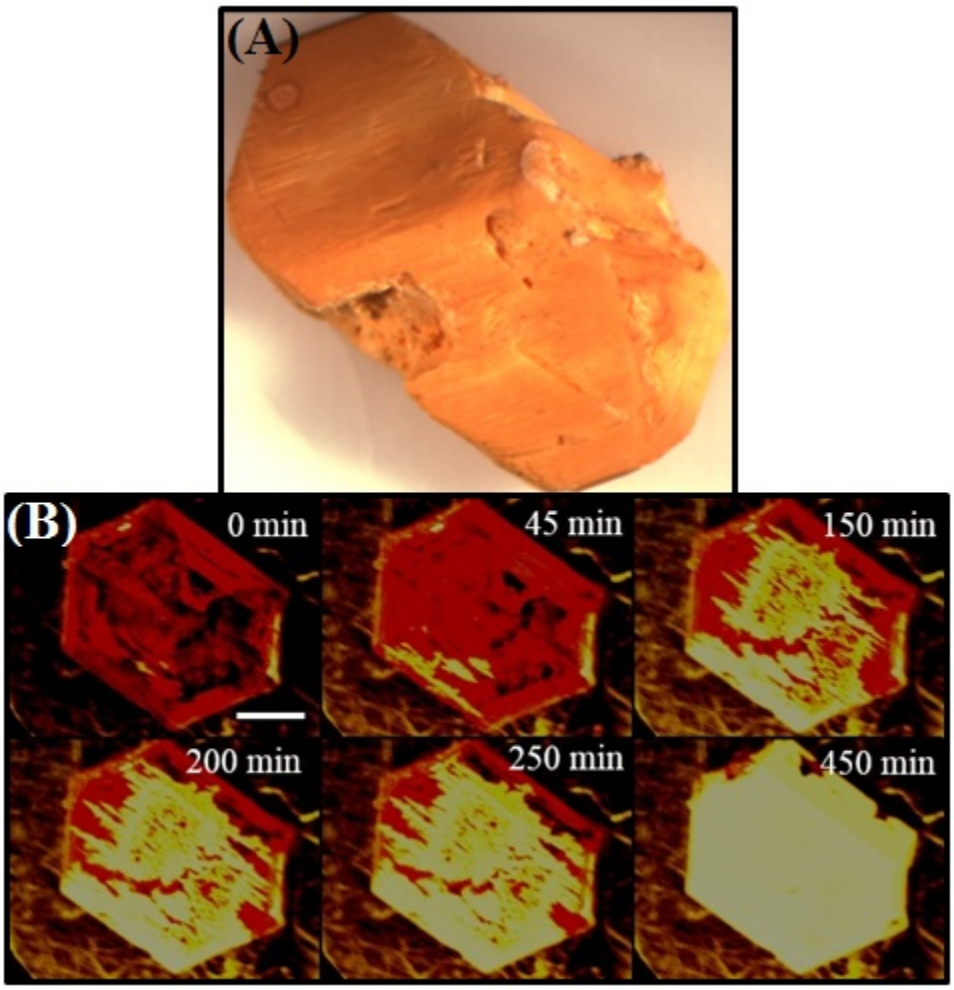

Figure 8. (A) Discoloration of the TNT/aniline cocrystal solvate after exposure to air (> 24 hours). The visual appearance of the crystal suggests that only TNT remains since pure crystals are typically brownish-yellow in appearance. (B) Macroscopic progression of the discoloration at the surface over a 9-hour period. The scale bar is 1 mm (images were taken with an optical microscope).

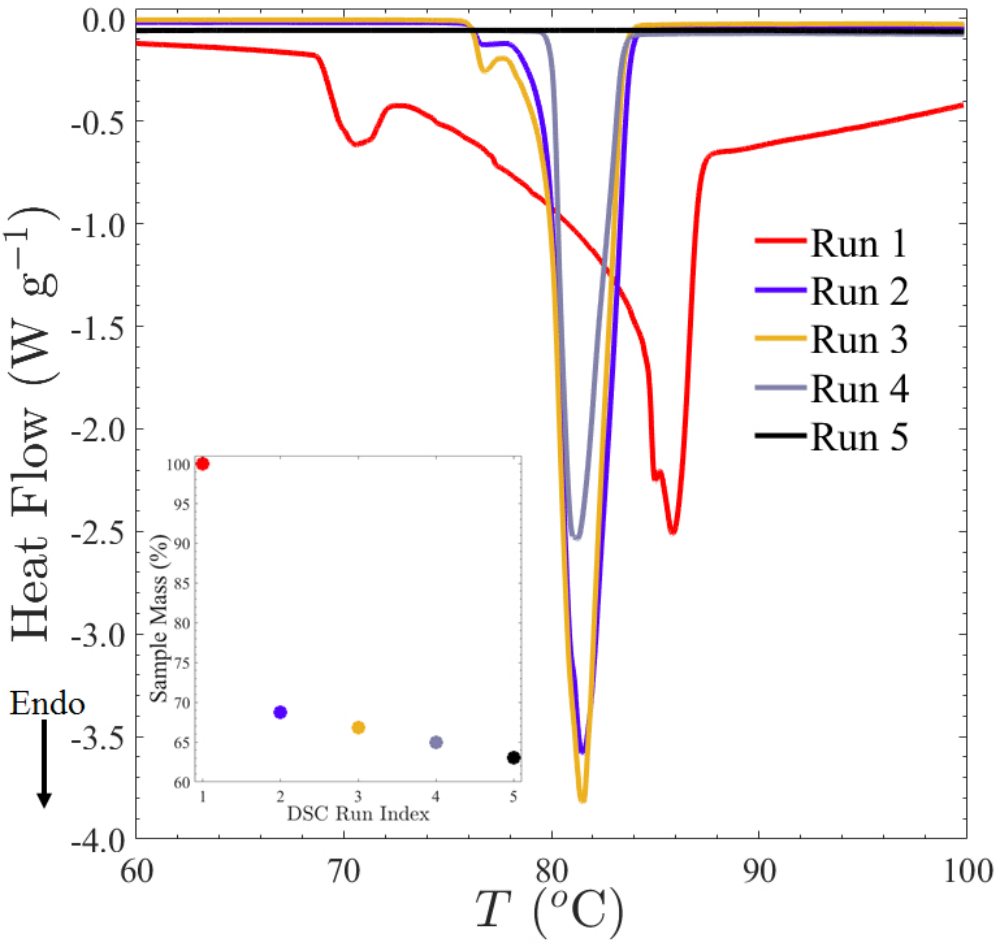

Figure 9. DSC traces (open-pan) for the same TNT/aniline cocrystal solvate sample after undergoing multiple heating and cooling (not shown) cycles up to slightly above the melting temperature. (Inset) The mass of the sample was subsequently measured after each respective cycle in which >30% was lost after the first run. The heating and cooling rates shown were both 5 oC min-1.

203x193mm (96 x 96 DPI)

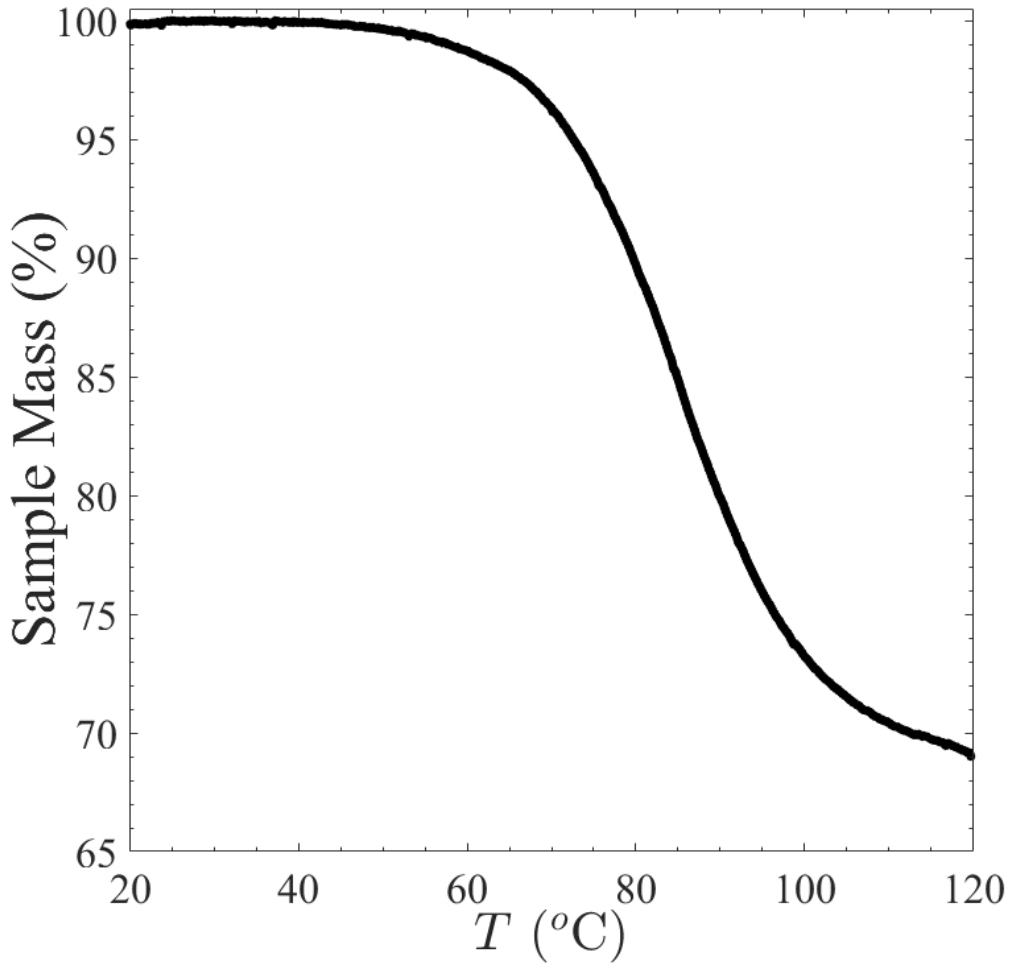

Figure 10. Non-isothermal TG results demonstrating the decrease in mass of a TNT/aniline cocrystal solvate sample when heated beyond the melting temperature. The heating rate was 20 oC min-1. Note: For 1:1 molar mixture of the two, aniline constitutes ~29% of the mass.

200x193mm (96 x 96 DPI)

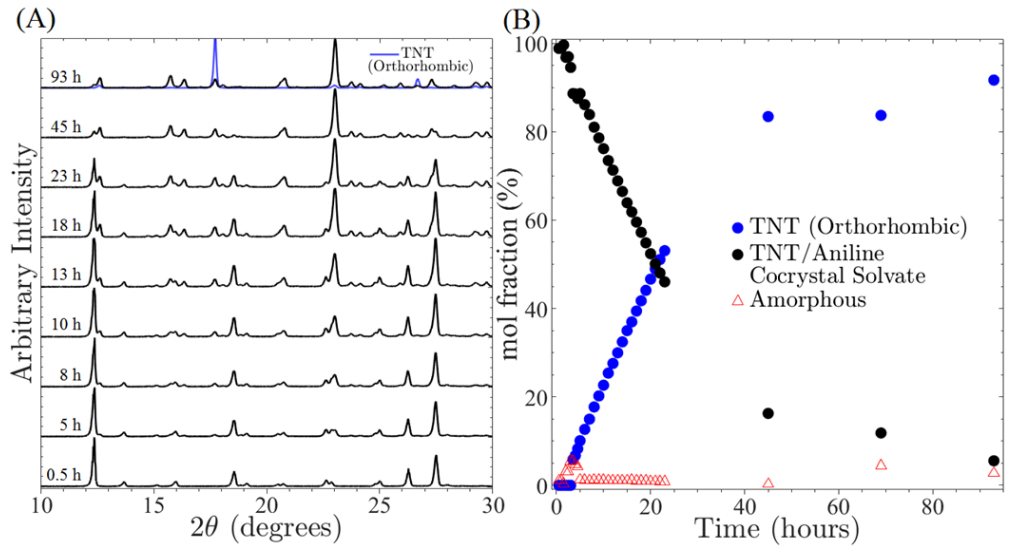

Figure 11. (A) A series of PXRD diffractograms of the TNT/aniline cocrystal solvate taken over time to monitor changes in the crystal structure under ambient conditions. (B) Time-dependent change in the crystal character as the cocrystal solvate converts into pure TNT due to aniline desolvation. The % composition was assessed by Rietveld analysis using the co-crystal solvate and the orthorhombic TNT polymorph as model patterns. During the analysis, it was determined that a small, amorphous component was also present throughout the crystal transition. Note: To demonstrate the conversion of the cocrystal solvate to TNT under ambient conditions, the sample was not repacked between measurements. This resulted in preferred orientation of the TNT crystals and slowed the conversion of the bottom portion of the sample.

278x152mm (96 x 96 DPI)

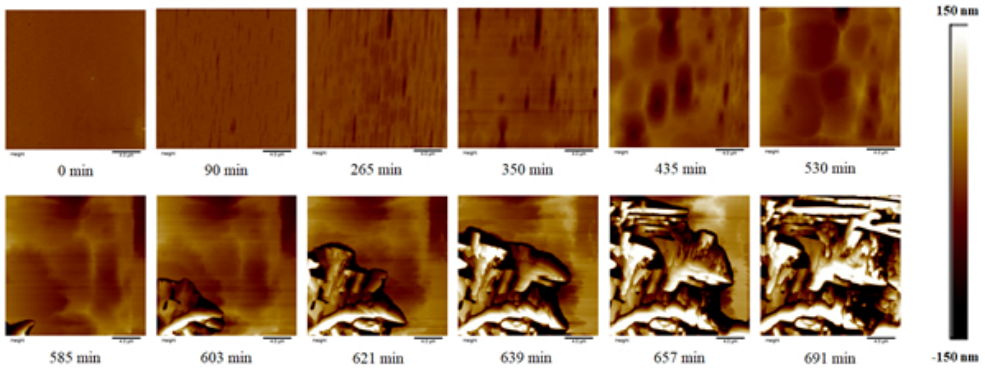

Figure 12. Evolution of AFM height images for the surface of a single TNT/aniline cocrystal solvate during isothermal heating at 35 oC. The top row shows growth of "pit" formations likely related to the desolvation of aniline. The bottom row shows an apparent reconstruction of the sample's surface into a different crystalline phase. All images are 20 μm ×20 μm2.

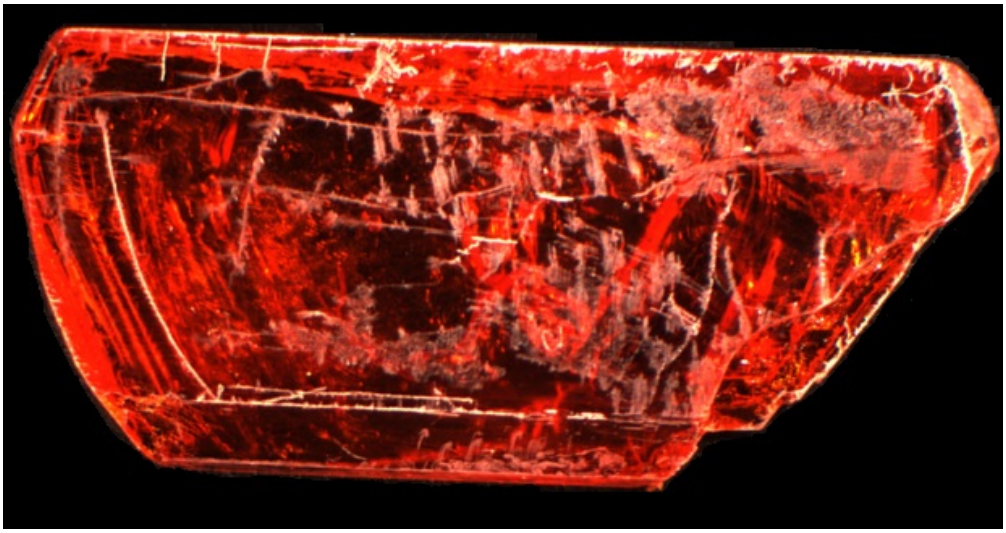

Table of Contents Graphics

163x85mm (96 x 96 DPI)